Journal of Sound and Vibration 330 (2011) 6098–6121

Contents lists available at ScienceDirect

Journal of Sound and Vibration

journal homepage: www.elsevier.com/locate/jsvi

Measurement of relevant elastic and damping material properties in sandwich thick plates

Marc Rébillat [a,b,*], Xavier Boutillon [a]

[a] Laboratoire de Mécanique des Solides (UMR CNRS 7649), École Polytechnique, 91128 Palaiseau Cedex, France
[b] Laboratoire d'Informatique pour la Mécanique et les Sciences de l'Ingénieur (UMR CNRS 3251), Université Paris-Sud, 91403 Orsay Cedex, France

ARTICLE INFO

Article history:
Received 18 December 2010
Received in revised form
19 May 2011
Accepted 13 July 2011
Handling Editor: K. Worden
Available online 19 August 2011

ABSTRACT

An easy-to-implement method to measure relevant elastic and damping properties of the constituents of a sandwich structure, possibly with a heterogeneous core, is proposed. The method makes use of a one-point dynamical measurement on a thick-plate. The hysteretic model for each (possibly orthotropic) constituent is written generically as "$E(1+j\eta)$" for all mechanical parameters. The estimation method of the parameters relies on a mixed experimental/numerical procedure. The frequencies and dampings of the natural modes of the plate are obtained from experimental impulse responses by means of a high-resolution modal analysis technique. This allows for considerably more experimental data to be used. Numerical modes (frequencies, dampings, and modal shapes) are computed by means of an extended Rayleigh–Ritz procedure under the "light damping" hypothesis, for given values of the mechanical parameters. Minimising the differences between the modal characteristics yields an estimation of the values of the mechanical parameters describing the hysteretic behaviour. A sensitivity analysis assesses the reliability of the method for each parameter. Validations of the method are proposed by (a) applying it to virtual plates on which a finite-element model replaces the experimental modal analysis, (b) some comparisons with results obtained by static mechanical measurements, and (c) by comparing the results on different plates made of the same sandwich material.

© 2011 Elsevier Ltd. All rights reserved.

1. Introduction

For plates having a mechanical function, sandwich structures, with possibly a heterogeneous core, are often preferred to a homogeneous constitutive material because they can be made lighter. However, the relevant mechanical properties of the sandwich as a whole or even of its individual components may be difficult to predict accurately, particularly when heterogeneous cores are used or if damping is considered. Here "*relevant*" refers to the parameters that matter in the plate dynamics (see Section 2.1). In this paper, a method for estimating the complex moduli of elasticity of the constituents of sandwich structures having a heterogeneous core based on one dynamical test on a plate is proposed. The proposed mixed experimental/numerical procedure (for an introduction to such procedures, see for example [1,2]) is based on the thick-plate model and frequency-independent mechanical properties of each constituent of the sandwich. It is intended to be easier to implement or to yield more parameters than other methods.

* Corresponding author at: Laboratoire de Mécanique des Solides (UMR CNRS 7649), École Polytechnique, 91128 Palaiseau Cedex, France. Tel.: +33 615971876.
E-mail address: marc.rebillat@polytechnique.edu (M. Rébillat).

0022-460X/$ - see front matter © 2011 Elsevier Ltd. All rights reserved.
doi:10.1016/j.jsv.2011.07.015

Using structural vibrations for the estimation of homogeneous material parameters is a widespread technique. Compared to static measurement campaigns which must be performed on a number of isolated samples of the sandwich components, dynamic tests leave the sandwich structure untouched and can be performed on one single panel of more or less arbitrary dimensions.

The problem of the estimation of solely *elasticity* parameters of a homogeneous material using plate vibrations has been widely addressed in a *thin-plate* context [1–7] and in a *thick-plate* context [8–21]. In a *thin-plate* context, only *in-plane* parameters can be estimated. Using a *thick-plate* yields some of the so-called *out-of-plane* parameters.

The problem of estimating *elasticity and damping* parameters of homogeneous materials by using point measurements [22–25] has retained some attention in a *thin-plate* context. In a *thick-plate* context, methods involving *full-field* measurements are currently available [26–28], but they are very time-consuming or need sophisticated equipment. Recently, some efforts have however been done to overcome these limitations by using point measurements instead of full-field measurements [29]. However, the experimental data used by these authors severely limits the possibilities of estimation, as discussed below.

For heterogeneous materials, such as sandwich materials, the literature addresses mainly the estimation of *elasticity* parameters, using either beams [30–32] or plates [33,34]. A few studies have been devoted in the last years to the problem of estimating their damping properties in beams [31,32], in plates by means of sophisticated full-field measurements [35,36], and quite recently in plates by single point measurements [37,38]. Since none of these studies present a sensitivity analysis, the validity of the model they used for damping is difficult to assess. The following reasoning explains how we access to significantly more experimental data than previous studies. The sensitivity analysis (Section 7) shows that these are determinant for some estimated parameters.

Exploiting the vibrations of sandwich panels with heterogeneous cores requires that the panel dimensions meet several conditions. In order to consider the sandwich core as homogeneous in the in-plane directions up to a given frequency f, the corresponding wavelength λ must contain at least 50 cells [39]. For a typical cell side-length s_{cell} and height h, this implies that the panel's dimensions are such that $l_{x,y} > \lambda > 50 s_{\text{cell}}$. Moreover *out-of-plane* elasticity and damping parameters can be estimated only on thick-enough plates. In brief, the panel must be large enough and the observed dynamics must include high-enough modes, within the limit of a plate model. Due to the intrinsic dissipation of materials, high-order modes may be impossible to characterise with methods based on the Fourier-transform (FT): those are limited to modal overlaps of $\mu \simeq 30$ percent in most implementations [35] (see Section 4.3 for the definition of μ). The high-resolution modal analysis (HRMA) technique recently developed by Ege et al. [40] is a successful substitute to the FT-based modal analysis techniques up to significantly higher modal overlap values.

From a methodological point of view, the present work is an extension to heterogeneous and thick plates of the work done by de Visscher et al. [23] on homogeneous thin plates. The proposed method is performed on large sandwich panels which meet the above conditions. Up to $\simeq 40$ modes are extracted by means of the HRMA. This is considerably more than the 6 or 12 modes used in [29] for the determination of six elastic parameters. It will be shown in Section 7 that high-frequency modes are indeed necessary for a reliable estimation of some of these parameters. As far as damping parameters are considered, experimental data used in [29] do not allow their reliable determination (as stated by the authors and confirmed by the sensitivity analysis in Section 7).

The mixed experimental/numerical procedure yielding the *in-plane* and most *out-of-plane* elasticity and damping parameters (complex elasticity moduli) of the constituents of the sandwich is schematically presented in Fig. 1. The analytical model of the sandwich panel is presented in Section 2. Based on this model, the numerical modal frequencies f_n^{Num} and dampings α_n^{Num} are derived by means of an extended Rayleigh–Ritz procedure (Section 3). The experimental protocol and the extraction method that yield the experimental modal frequencies f_n^{XP} and dampings α_n^{XP} are presented in Section 4. Given the numerical and experimental data, the optimisation procedure that estimates elasticity and damping parameters of the constituents of the sandwich material is detailed in Section 5. The procedure is validated in Section 6 by

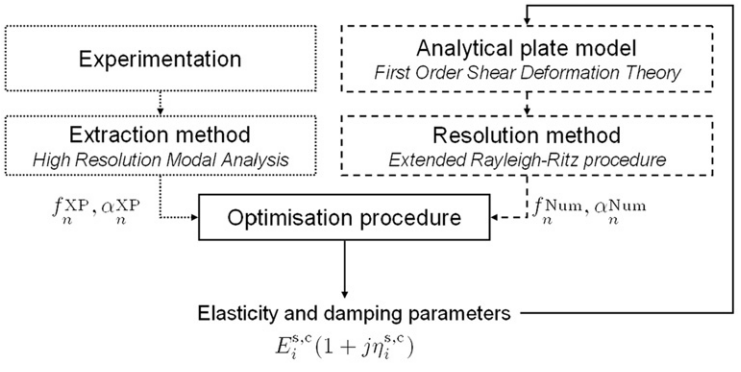

Fig. 1. Overview of the proposed mixed experimental/numerical procedure: modal characteristics derived experimentally and numerically are compared; their differences tend to zero when the correct values of the mechanical parameters are reached.

means of a finite-element analysis. Measurements performed on three real plates are shown in Section 7 which provides additional validation insight as well.

2. A mechanical model of sandwich panels

In order to access the modal dampings and frequencies of a sandwich panel, an adapted mechanical model is needed. In this section, such a complex structure is modelled as an equivalent thick-plate under the Reissner–Mindlin hypothesis. A frequency-independent model for the materials composing the sandwich is also described. Notations used in this section are summarised by Tables D1, D2 and D3 in Appendix D.

2.1. Hypothesis

The sandwich panel consists of two identical skins and a core (Fig. 2). The thicknesses of the core, skins, and panel are h^c, h^s, and $h=h^c+2h^s$ respectively. In the following, "panel" designates the physical structure whereas "plate" refers to the idealised structure made out of the equivalent homogeneous material. The following hypotheses are made on the panel and plate:

- Displacements are small so that the materials and structures behave linearly.
- Only flexural waves of frequencies far from the delamination frequency (the frequency of the first transverse mode of the panel) are considered.
- The plate is considered to follow the Reissner–Mindlin approximations (thick-plate: first-order shear deformation theory, FSDT), with no direct strain in the z-direction. As pointed out by Refs. [41–43], the accuracy of the thick-plate model to describe the dynamics of sandwich plates having a soft core depends mainly on the thickness to length ratio and on the skins Young modulus to core shear modulus ratio: $E^s_{x,y}/G^c_{yz,xz}$. Generally, the thicker and the softer the core, the less the thick-plate model is appropriate for modelling purposes as compared to higher-order models. In [42, Fig. 4], a comparison between thick-plate theory (FSDT) and high-order shear deformation theory (HSDT) is performed on the first modal frequency of a sandwich panel with a soft core. At least for orders of magnitude considered, it could be extended to a higher modal frequency of wavelength λ by considering the ratio $2h/\lambda$ instead of $h/l_{x,y}$ (the "h" written here is defined in Fig. 2 and corresponds to the writing "$2h$" in [42]). According to [42, Fig. 4(c) and (d)], the difference between FSTD and HSDT does not exceed 5 percent for $E^s_{x,y}/G^c_{yz,xz}\simeq 100$ and a $2h/\lambda$ ratio less than 0.08. The plates that are considered in this paper exhibit a $E^s_{x,y}/G^c_{yz,xz}\simeq 100$ ratio and the highest modes under consideration are characterised by $2h/\lambda\simeq 0.08$. A thick-plate model based on FSDT is thus appropriate enough in the present study.
- The wavelengths λ include at least 50 cells. According to Burton et al. [39], this ensures that errors on the modal frequencies of the plate (with a homogeneous equivalent core) are less than 2 percent when compared to those of the panel as computed by various finite-elements models.

The skin and core materials are considered as homogeneous, orthotropic in the x- and y-directions.

The formalism chosen for describing the hysteretic behaviour is that of complex moduli $\underline{E}=E(1+j\eta)$ which do not depend on the frequency (see the model of materials in Section 2.2). Young's and shear moduli and the Poisson coefficient of the core are $\underline{E}^c_x$, $\underline{E}^c_y$, $\underline{E}^c_z$, $\underline{G}^c_{xy}$, $\underline{G}^c_{xz}$, $\underline{G}^c_{yz}$, $\underline{\nu}^c_{yx}$, $\underline{\nu}^c_{xz}$, $\underline{\nu}^c_{yz}$ and $\underline{\nu}^c_{xy}$. The same parameters for the skins are denoted by the index "s". The properties of the homogeneous material equivalent to the whole sandwich are denoted by the index "H". Additional symmetry relationships are given in Section 2.2.

The following hypotheses are made on the sandwich panel:

- The sandwich panel is symmetric with respect to its mid-plane.
- Skins are thin compared to the core and the core is softer than the skins so that shear stress in the skins can be ignored: $h^s/G^s_{xz}\ll h^c/G^c_{xz}$ (and the same in the y-direction).

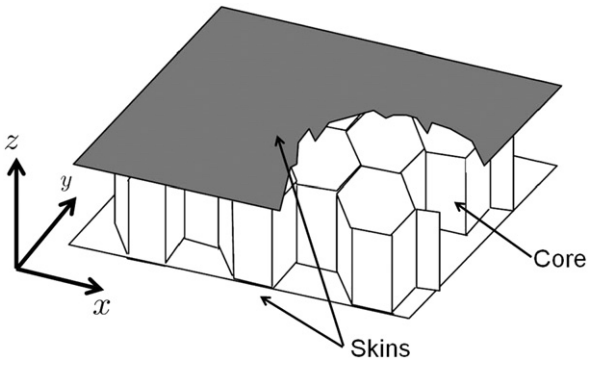

Fig. 2. Geometry of the sandwich plate.

- The core is very soft ($E_x^c \ll E_x^s$, $E_y^c \ll E_y^s$ and $G_{xy}^c \ll G_{xy}^s$). Given the generic expression of the moduli of the homogeneous equivalent material $E^H = (h^c/h)^3 E^c + [1-(h^c/h)^3]E^s$, this ensures that all in-plane stress in the plate are entirely due to those in the skins.

According to these hypotheses, there is no stress associated with $\underline{E}_z^{c,s,H}$, $\underline{\nu}_{xz}^{c,s,H}$, $\underline{\nu}_{yz}^{c,s,H}$, $\underline{G}_{xz}^s$, $\underline{G}_{yz}^s$, $\underline{E}_x^c$, $\underline{E}_y^c$, $\underline{G}_{xy}^c$, $\underline{\nu}_{xy}^c$, $\underline{\nu}_{yx}^c$ which are ignored in what follows. The relevant remaining mechanical parameters describing such a plate are thus [36]:

- *In-plane* parameters (bending of the skins): $\underline{E}_x^s$, $\underline{E}_y^s$, $\underline{G}_{xy}^s$, $\underline{\nu}_{yx}^s$, $\underline{\nu}_{xy}^s$.
- *Out-of-plane* parameters (shearing in the core) : $\underline{G}_{xz}^c$, $\underline{G}_{yz}^c$ (excluding $\underline{E}_z^c$).

In the rest of the article, it will thus be understood that "*elastic parameters*" means "*relevant elastic parameters for the dynamics of thick-plates*".

These hypotheses are generally fulfilled in common sandwich panels. Typical orders of magnitude for parameters are:

$$\begin{cases} h^s/h^c \simeq 10^{-1} \\ E_x^c/E_x^s \simeq E_y^c/E_y^s \simeq G_{xy}^c/G_{xy}^s \simeq 10^{-4} \end{cases} \tag{1}$$

2.2. Model of the materials

The damping of plate vibrations has different origins. In the present study, it is assumed that panels vibrate below their coincidence acoustical frequencies [44]. Consequently, damping due to acoustical radiation in surrounding air is very small compared to the structural damping [45]. Among the different structural damping models, the standard hysteretic model (which is frequency-independent, see for example [46,47]) has been retained. The relationship between the stress $\boldsymbol{\varepsilon}^\gamma$ and the strain $\boldsymbol{\sigma}^\gamma$ in each γ-material ($\gamma = s,c$, or H) involves seven complex numbers and can be written, to first order in η^γ, as

$$\boldsymbol{\sigma}^\gamma = \begin{bmatrix} E_x^\gamma(1+\mathrm{j}\eta_x^\gamma) & \nu_{yx}^\gamma E_x^\gamma[1+\mathrm{j}(\eta_{\nu_{yx}}^\gamma+\eta_x^\gamma)] & 0 & 0 & 0 \\ \nu_{xy}^\gamma E_y^\gamma[1+\mathrm{j}(\eta_{\nu_{xy}}^\gamma+\eta_y^\gamma)] & E_y^\gamma(1+\mathrm{j}\eta_y^\gamma) & 0 & 0 & 0 \\ 0 & 0 & G_{xz}^\gamma(1+\mathrm{j}\eta_{xz}^\gamma) & 0 & 0 \\ 0 & 0 & 0 & G_{yz}^\gamma(1+\mathrm{j}\eta_{yz}^\gamma) & 0 \\ 0 & 0 & 0 & 0 & G_{xy}^\gamma(1+\mathrm{j}\eta_{xy}^\gamma) \end{bmatrix} \boldsymbol{\varepsilon}^\gamma \tag{2}$$

The symmetry of the strain/stress relation adds the following relationships $\nu_{xy}^\gamma E_y^\gamma = \nu_{yx}^\gamma E_x^\gamma$ and $\eta_\nu^\gamma = \eta_{\nu_{xy}}^\gamma + \eta_y^\gamma = \eta_{\nu_{yx}}^\gamma + \eta_x^\gamma$ which leaves 12 independent real parameters to be identified for each material (24 altogether).

2.3. Equivalent thick-plate

Under the hypothesis and for the orders of magnitude given in Section 2.1, the sandwich panel behaves in the low-frequency range like a homogeneous thick-plate [48]. The thickness of the plate is chosen to be h. Its mechanical properties are given in Eqs. (3) and (4) as functions of the mechanical and geometrical properties of the skins and the core:

$$\begin{cases} E_x^H = E_x^s\left[1-\left(\dfrac{h^c}{h}\right)^3\right], \quad E_y^H = E_y^s\left[1-\left(\dfrac{h^c}{h}\right)^3\right], \quad \nu_{xy}^H = \nu_{xy}^s \\ G_{xy}^H = G_{xy}^s\left[1-\left(\dfrac{h^c}{h}\right)^3\right], \quad G_{xz}^H = G_{xz}^c, \quad G_{yz}^H = G_{yz}^c \end{cases} \tag{3}$$

$$\begin{cases} \eta_x^H = \eta_x^c \dfrac{E_x^c}{E_x^s}\left(\dfrac{h^c}{h}\right)^3 + \eta_x^s\left[1-\left(\dfrac{h^c}{h}\right)^3\right], \quad \eta_y^H = \eta_y^c \dfrac{E_y^c}{E_y^s}\left(\dfrac{h^c}{h}\right)^3 + \eta_y^s\left[1-\left(\dfrac{h^c}{h}\right)^3\right] \\ \eta_{xy}^H = \eta_{xy}^c \dfrac{G_{xy}^c}{G_{xy}^s}\left(\dfrac{h^c}{h}\right)^3 + \eta_{xy}^s\left[1-\left(\dfrac{h^c}{h}\right)^3\right], \quad \eta_{xz}^H = \eta_{xz}^c, \quad \eta_{yz}^H = \eta_{yz}^c, \quad \eta_\nu^H = \eta_\nu^s \end{cases} \tag{4}$$

The 12 independent real parameters $\{E_x^H, \eta_x^H, E_y^H, \eta_y^H, G_{xy}^H, \eta_{xy}^H, G_{xz}^H, \eta_{xz}^H, G_{yz}^H, \eta_{yz}^H, \nu_{xy}^H, \eta_\nu^H\}$ are to be estimated. Their knowledge yields the elastic and damping properties of each layer of the sandwich panel provided that the 12-equation system formed by Eqs. (3) and (4) is invertible. A sufficient condition is

$$\eta_x^c \frac{E_x^c}{E_x^s} \ll \eta_x^s, \quad \eta_y^c \frac{E_y^c}{E_y^s} \ll \eta_y^s, \quad \eta_{xy}^c \frac{G_{xy}^c}{G_{xy}^s} \ll \eta_{xy}^s \tag{5}$$

since $E_x^c/E_x^s \ll 1$, $E_y^c/E_y^s \ll 1$, and $G_{xy}^c/G_{xy}^s \ll 1$ (see Section 2.1). This condition is not satisfied only if the η^c-coefficients are several orders of magnitude larger than the η^s-ones. This is not the case here and rarely the case in general.[1] Consequently, the estimation of E_x^H, *etc.* yields an estimation of the mechanical properties of the skin and core materials.

2.4. Potential, kinetic and dissipated energies in the equivalent thick-plate

Within the frame of the first-order Reissner–Mindlin theory [49, Chapter 3], the displacements $\{u,v,w\}$ in the $\{x, y, z\}$-directions respectively can be written within a good approximation (see below) as

$$u(x,y,z) = -z\Phi_x(x,y), \quad v(x,y,z) = -z\Phi_y(x,y), \quad w(x,y,z) = w_0(x,y) \tag{6}$$

The potential energy of the plate is

$$\begin{aligned} U &= \frac{1}{2}\iiint_{\mathcal{V}} (\boldsymbol{\sigma}^H)^T \boldsymbol{\varepsilon}^H \, \mathrm{d}\tau \\ &= \frac{1}{2}\iint_{\mathcal{S}} \left[D_1\left(\frac{\partial\Phi_x}{\partial x}\right)^2 + D_2\left(\frac{\partial\Phi_x}{\partial x}\frac{\partial\Phi_y}{\partial y}\right) + D_3\left(\frac{\partial\Phi_y}{\partial y}\right)^2 + D_4\left(\Phi_y^2 - 2\Phi_y\frac{\partial w_0}{\partial y} + \left(\frac{\partial w_0}{\partial y}\right)^2\right) \right. \\ &\left. + \cdots + D_5\left(\Phi_x^2 - 2\Phi_x\frac{\partial w_0}{\partial x} + \left(\frac{\partial w_0}{\partial x}\right)^2\right) + D_6\left(\left(\frac{\partial\Phi_x}{\partial y}\right)^2 + 2\frac{\partial\Phi_x}{\partial y}\frac{\partial\Phi_y}{\partial x} + \left(\frac{\partial\Phi_y}{\partial x}\right)^2\right)\right] \mathrm{d}x\,\mathrm{d}y \end{aligned} \tag{7}$$

with

$$D_1 = \frac{E_x^H h^3}{12(1-\nu_{xy}\nu_{yx})}, \quad D_2 = \frac{\nu_{xy}E_y^H h^3}{6(1-\nu_{xy}\nu_{yx})}, \quad D_3 = \frac{E_y^H h^3}{12(1-\nu_{xy}\nu_{yx})}$$

$$D_4 = 2\kappa_{yz}^2 h G_{yz}^H, \quad D_5 = 2\kappa_{xz}^2 h G_{xz}^H, \quad D_6 = \frac{G_{xy}^H h^3}{6} \tag{8}$$

The shear correction factors κ_{yz}^2 and κ_{xz}^2 account for the fact that Eq. (6) is an approximation: the (functional) angles Φ_x and Φ_y depend lightly on z and sections of the plate do not remain plane in the flexural deformation. The values $\kappa_{yz} = \kappa_{xz} = 1$ have been chosen according to the recommendations of [50] for sandwich panels.

By definition, the fraction of energy lost during one cycle $\mathcal{T}$ is

$$\Delta U = -\int_{\mathcal{T}} \left[\iiint_{\mathcal{V}} (\boldsymbol{\sigma}^H)^T \frac{\partial \boldsymbol{\varepsilon}^H}{\partial t} \, \mathrm{d}\tau\right] \mathrm{d}t \tag{9}$$

Based on Section 2.2, ΔU can then be expressed as

$$\begin{aligned} \Delta U = -\pi \iint_{\mathcal{S}} &\left[\eta_x^H D_1\left(\frac{\partial\Phi_x}{\partial x}\right)^2 + \eta_v^H D_2\left(\frac{\partial\Phi_x}{\partial x}\frac{\partial\Phi_y}{\partial y}\right) + \eta_y^H D_3\left(\frac{\partial\Phi_y}{\partial y}\right)^2 + \eta_{yz}^H D_4\left(\Phi_y^2 - 2\Phi_y\frac{\partial w_0}{\partial y} + \left(\frac{\partial w_0}{\partial y}\right)^2\right)\right. \\ &\left. + \cdots + \eta_{xz}^H D_5\left(\Phi_x^2 - 2\Phi_x\frac{\partial w_0}{\partial x} + \left(\frac{\partial w_0}{\partial x}\right)^2\right) + \eta_{xy}^H D_6\left(\left(\frac{\partial\Phi_x}{\partial y}\right)^2 + 2\frac{\partial\Phi_x}{\partial y}\frac{\partial\Phi_y}{\partial x} + \left(\frac{\partial\Phi_y}{\partial x}\right)^2\right)\right] \mathrm{d}x\,\mathrm{d}y \end{aligned} \tag{10}$$

The kinetic energy T of the system is given in Eq. (11) as a function of Φ_x, Φ_y, and w_0. In this expression, ρ^H is the density of the equivalent homogeneous thick-plate. It is given by $h\rho^H = h^c\rho^c + 2h^s\rho^s$.

$$T = \frac{\rho^H\omega^2}{2}\iiint_{(\mathcal{V})} [u^2 + v^2 + w^2] \, \mathrm{d}\tau = \frac{\rho^H\omega^2}{2}\iint_{(\mathcal{S})} \left[\frac{h^3}{12}(\Phi_x^2 + \Phi_y^2) + h w_0^2\right] \mathrm{d}x\,\mathrm{d}y \tag{11}$$

3. Estimation of modal parameters by an extended Rayleigh–Ritz procedure

In order to compare experimental results to numerical simulations, it is necessary to evaluate the frequencies f_n^{Num} and damping factors α_n^{Num} of the numerical modes corresponding to the sandwich panel. The dynamics of the plate is given by the hypotheses listed in Section 2.1, by Eqs. (2), and by the boundary conditions. Under the "light damping" hypothesis, which assumes that modal shapes and frequencies are unchanged by the addition of damping, the frequencies f_n^{Num} of the numerical modes are easily accessible. The problem consists thus in evaluating the relationships between the α_n^{Num} damping factors and the η^H loss-factors. Notations used in this section are summarised by Table D4 in Appendix D.

[1] It can be the case when skins are made of metal and the core is made of paper honeycombs or of viscoelastic foam.

3.1. Light damping hypothesis

The honeycomb sandwich panel is considered here as a non-conservative system $\mathcal{P}_{NC}$ having N degrees of freedom. The associated conservative system, without hysteretic damping and having also N degrees of freedom, is denoted by $\mathcal{P}_C$. The N modes of $\mathcal{P}_C$ have their modal shapes denoted by ξ_n^C and their real modal frequencies denoted by f_n^C. The N modes of $\mathcal{P}_{NC}$ have their modal shapes denoted by ξ_n^{NC} and their complex modal frequencies denoted by f_n^{NC}.

If $\mathcal{P}_{NC}$ is lightly damped, it can be shown [51] that $\xi_n^{NC} \simeq \xi_n^C$ and that $f_n^{NC} \simeq f_n^C + j\alpha_n$ to first order. The "light damping" hypothesis thus assumes that modal shapes and real parts of the frequencies are unchanged by the addition of damping. This hypothesis has been shown to be acceptable for values of material loss factors lower than 0.1 [52]. This assumption is similar to the assumption made in the "Modal Strain Energy" approach used to model sandwich panels having visco-elastic cores [52–54].

Let U_n^{NC} be the potential energy associated with the nth mode of $\mathcal{P}_{NC}$ for a maximum vibrational amplitude of 1 on the plate. It varies in time as $\exp(-2\alpha_n t)$ so that the energy lost by this mode during one cycle, ΔU_n^{NC}, is

$$\Delta U_n^{NC} = -2\frac{\alpha_n}{f_n^C} U_n^{NC} \tag{12}$$

Since $\mathcal{P}_C$ and $\mathcal{P}_{NC}$ have the same modal shapes, *i.e.* $\xi_n^{NC} \simeq \xi_n^C$, and the potential energy depends only on the modal shapes (see Eq. (7)), then $U_n^{NC} = U_n^C$. And since for the conservative system $\mathcal{P}_{NC}$, the equality $U_n^C = T_n^C$ is true, one then obtains

$$\Delta U_n^{NC} = -2\frac{\alpha_n}{f_n^C} T_n^C \tag{13}$$

Thanks to the light damping hypothesis, Eq. (13) gives a straightforward way to obtain the modal dampings α_n from ΔU_n^{NC}, T_n^C and, f_n^C.

3.2. Derivation of f_n^{Num}

A Rayleigh–Ritz procedure has been used to derive numerically the modal frequencies f_n^{Num} and the mode shapes ξ_n^{Num} of $\mathcal{P}_C$. To this end, the generalised-displacement fields $\Phi_x(x,y)$, $\Phi_y(x,y)$, and $w_0(x,y)$ are projected on the elements of an orthonormal polynomial basis of order Q satisfying partially the free–free boundary conditions [55,56]:

$$\Phi_x(x,y) = \sum_{i,j} L_{ij} p_i(x) p_j(y), \quad \Phi_y(x,y) = \sum_{i,j} M_{ij} p_i(x) p_j(y), \quad w_0(x,y) = \sum_{i,j} N_{ij} p_i(x) p_j(y) \tag{14}$$

where the polynomials $p_i(\kappa)$ are generated as described in Appendix A.

This procedure generates a new set of $3Q^2$ generalised displacements L_{ij}, M_{ij} and N_{ij}. The next step consists in writing the kinetic and potential energies T and U which have been expressed as functions of Φ_x, Φ_y, and w_0 in Section 2.4. The Hamilton principle reads as

$$\forall (i,j) \in [0,Q-1]^2 : \ \frac{\partial(T-U)}{\partial L_{ij}} = 0, \quad \frac{\partial(T-U)}{\partial M_{ij}} = 0, \quad \frac{\partial(T-U)}{\partial N_{ij}} = 0 \tag{15}$$

The above system of $3Q^2$ linear equations can be re-written as $[\boldsymbol{K} - 4\pi^2 f^2 \boldsymbol{M}]\boldsymbol{q} = 0$. The expressions of the partial derivatives of U with respect to L_{ij},M_{ij},N_{ij} yield $\boldsymbol{K}$ while the partial derivatives of T with respect to L_{ij},M_{ij},N_{ij} yield $\boldsymbol{M}$. The explicit expressions for these partial derivatives as functions of the p_i's and of the generalised displacements are given in Appendix B. The resolution of this eigenvalue problem gives a straightforward access to the modal frequencies f_n^{Num} and mode shapes ξ_n^{Num} of $\mathcal{P}_C$. Under the light damping hypothesis, ξ_n^{Num} and f_n^{Num} found for $\mathcal{P}_C$ are also the modal shapes and frequencies of $\mathcal{P}_{NC}$ (see Section 3.1).

3.3. Derivation of α_n^{Num}

Introducing the modal coefficients ξ_n^{Num} (expressed in the $\{L_{ij},M_{ij},N_{ij}\}$ system of coordinates) into Eqs. (14) yields analytical expressions for the Φ_x, Φ_y, and w_0 modal fields and also for their x- and y-derivatives. For each of the N modes, the potential, lost, and kinetic energies can be written by introducing these expressions into Eqs. (7), (10) and (11):

$$\forall n \in [1,N] : \quad T_n^C = 4\pi^2 (f_n^{Num})^2 t_n, \quad U_n^{NC} = U_n^C = \sum_{k=1}^{6} D_k u_k^n, \quad \Delta U_n^{NC} = -\pi \sum_{k=1}^{6} \eta_k D_k u_k^n \tag{16}$$

where the subscripts $\{1,2,3,4,5,6\}$ of η stand for $\{x,v,y,yz,xz,xy\}$ respectively. The coefficients t_n and u_k^n are given explicitly in Appendix C. They depend on the geometry and mass parameters of the plate, and are quadratic in modal shapes ξ_n^{Num}. Note that t_n can be considered as half the modal mass for some normalised displacement. The product $D_k u_k^n$ represents the k-contribution to the nth modal stiffness (where k stands for x, v, y, yz, xz, or xy).

The expression (17) of the modal dampings α_n^{Num} can be deduced from Eq. (13) and the last two expressions of (16) or, equivalently, by (12) and the first two expressions of (16):

$$\alpha_n^{\mathrm{Num}} = -\frac{f_n^{\mathrm{Num}}\Delta U_n^{NC}}{2T_n^C} = \frac{1}{8\pi f_n^{\mathrm{Num}} t_n}\sum_{k=1}^{6}\eta_k D_k u_k^n \quad \text{or} \quad \alpha_n^{\mathrm{Num}} = -\frac{f_n^{\mathrm{Num}}\Delta U_n^{NC}}{2U_n^C} = \frac{f_n^{\mathrm{Num}}\pi}{2\sum_{m=1}^{6} D_m u_m^n}\sum_{k=1}^{6}\eta_k D_k u_k^n \tag{17}$$

One can notice that α_n^{Num} is a linear combination of the η_k. This set of equations is a generalisation to all the modes of a thick-plate of the expression given by de Visscher et al. [23, Eq. (13)] for three particular modes of a thin plate. This expression is also a generalisation to all the loss factors of the expression established by Johnson et al. [53] for sandwich structures having a visco-elastic core.

4. Estimation of modal parameters by high-resolution modal analysis

In this section, the experimental protocol that has been followed to obtain impulse responses and to extract the modal frequencies f_n^{XP} and the damping factors α_n^{XP} is presented. This protocol combines the procedures and implementation details presented by Rébillat et al. [57,58] and Ege et al. [40].

4.1. Experimental setup

Throughout all measurements, panels were suspended by thin wires in order to ensure free–free boundary conditions. Light panels were acoustically excited by an electro-dynamical loudspeaker driven by a wide-band electrical signal [27]. The velocity response was measured in one corner of each panel with a laser Doppler vibrometer (Ometron VH300+ type 8329). Eventual nonlinearities arising from the loudspeaker were removed and the impulse response of the panel was reconstructed [57,58]. Since heavy panels can hardly be excited by acoustical means, impact excitations were also used; in this case, the acceleration resulting from the impact was recorded with a light accelerometer fixed in the vicinity of one corner of the panel. The impulse response was obtained after deconvolution with the nearly impulsive force signal [40]. Since no nodal line goes through corners of a free vibrating plate, all excited modes contribute to the resulting impulse response.

4.2. High-resolution modal analysis

It is hypothesised that the experimental data are corrupted by additive noise. Thus, an impulse response $h(t)$ is mathematically represented as a sum of decaying exponentials (natural modes) and measurement noise $b(t)$ as in Eq. (18). Each contribution of a natural mode is characterised by its amplitude A_n^{XP}, frequency f_n^{XP}, damping α_n^{XP} and phase ϕ_n^{XP}:

$$\begin{aligned} h(t) &= \sum_{n=1}^{N} A_n^{\mathrm{XP}}\exp(-\alpha_n^{\mathrm{XP}}t)\cos(2\pi f_n^{\mathrm{XP}}t+\phi_n^{\mathrm{XP}})+b(t) \\ &= \sum_{n=1}^{N}\frac{A_n^{\mathrm{XP}}}{2}[\exp(-\alpha_n^{\mathrm{XP}}t+j2\pi f_n^{\mathrm{XP}}t+\mathrm{j}\phi_n^{\mathrm{XP}})+\exp(-\alpha_n^{\mathrm{XP}}t-j2\pi f_n^{\mathrm{XP}}t-\mathrm{j}\phi_n^{\mathrm{XP}})]+b(t) \end{aligned} \tag{18}$$

In order to extract experimental modal frequencies f_n^{XP} and damping α_n^{XP} from $h(t)$, the recently developed "high resolution modal analysis" (HRMA) [40] has been applied and is briefly sketched below. The signal is projected onto two subspaces: the subspace spanned by the sinusoids (*signal subspace*) and its supplementary (*noise subspace*) according to the ESPRIT (Estimation of Signal Parameters via Rotational Invariance Techniques) algorithm [59]. The frequencies f_n^{XP} and

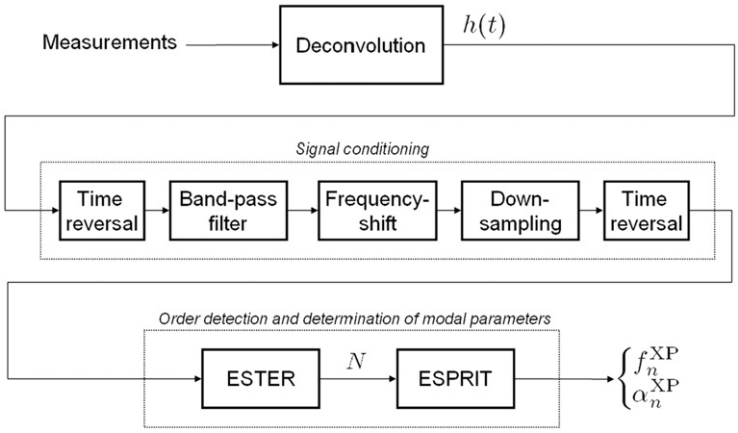

Fig. 3. Block diagram of the high-resolution modal analysis method, adapted from [40]. The deconvolution block is described in [57].

dampings α_n^{XP} of a given number of modes are the eigenvalues of a matrix obtained after some computation on the observed signal. The amplitudes A_n^{XP} and phases ϕ_n^{XP} are estimated afterwards by a least-mean-square method.

In the ESPRIT procedure, the dimensions of both subspaces must be chosen *a priori* and the quality of the estimation significantly relies on a proper choice for these parameters. The best choice for the dimension of the signal subspace is the number of exponentials (twice the number of decaying sinusoids, or real modes, see Eq. (18)). This number can be estimated, before the analysis, by means of the ESTER technique [60].

To improve the performance of the ESPRIT algorithm, signals are split into several frequency-bands [61], thus reducing the number of modes to be processed. In order to limit computation time, the responses of the band-pass filters are frequency-shifted and down-sampled.

A block-diagram describing the different steps involved in HRMA is shown in Fig. 3.

4.3. Uncertainties in modal parameters estimation

To give an overview of the precision offered by the HRMA, this method is applied to a synthetic signal obtained by adding two decaying exponentials of equal amplitudes to white noise. The sampling frequency is $f_s = 44.1$ kHz. The two modal frequencies are 592 and 596 Hz, very close one from each other. For relatively important modal dampings, these two modes overlap in the frequency-domain and therefore, their frequencies and dampings are difficult to estimate with methods based on the Fourier transform (FT). The modal overlap factor μ (*i.e.* the ratio between the half-power modal bandwidth $\Delta f_{-3\,\mathrm{dB}}$ and the average modal spacing Δf_{mode}) quantifies this phenomenon [40]. If the modal damping α is the same for both modes μ is

$$\mu = \frac{1}{\Delta f_{\mathrm{mode}}} \frac{\alpha}{\pi} \tag{19}$$

In practice, the FT cannot efficiently separate modes when $\mu > 30$ percent [35]. For HRMA, this upper limit depends on the signal/noise ratio and on the number of components which are retained in the pre-conditioning step. As an example,

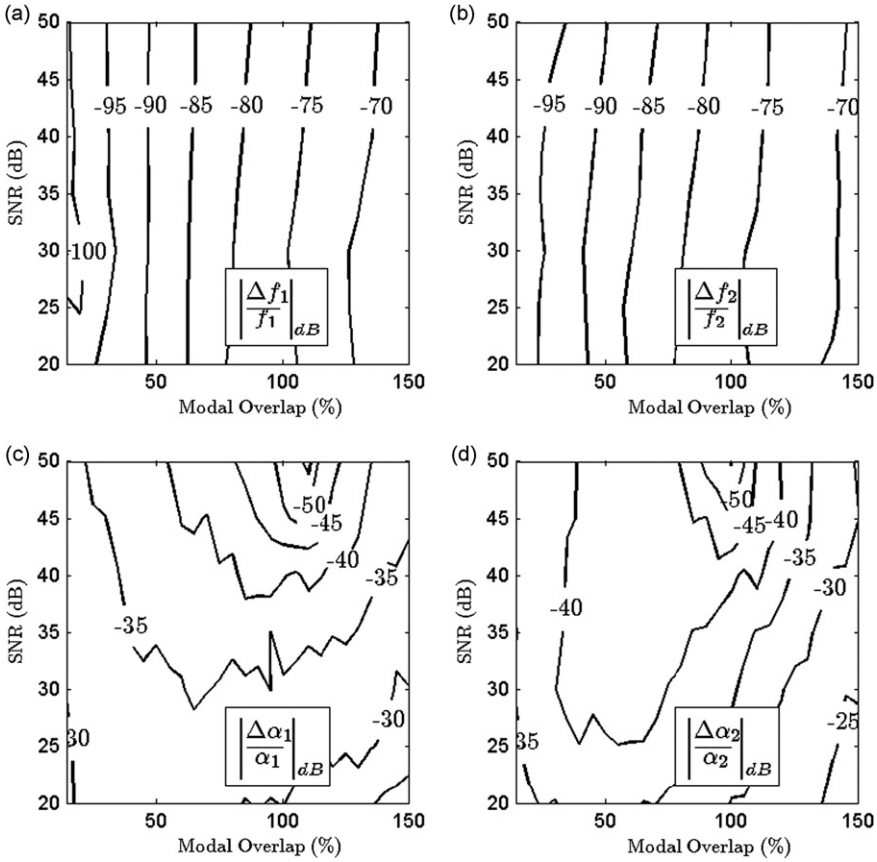

Fig. 4. Contour plots of the uncertainty on the estimated "modal" frequencies and dampings of a synthetic signal containing two decaying sinusoids as a function of the modal overlap and the signal-to-noise ratio. The uncertainty is the mean of 50 absolute values of the relative error between original and estimated data, for 50 different realisations of the noise. (a) Uncertainties on the frequency of the first mode. (b) Uncertainties on the frequency of the second mode. (c) and (d) *idem* relatively to the dampings.

estimations of modal frequencies and dampings have been performed on the synthetic signal with various α-values (corresponding to modal overlaps from $\mu=1$ percent to 150 percent) and a signal-to-noise ratio (SNR) increasing from 20 dB to 50 dB. SNR is understood here as $20\log_{10}(S_{\mathrm{RMS}}/B_{\mathrm{RMS}})$, where S_{RMS} is the RMS value of signal in the absence of noise and B_{RMS} the RMS value of noise in absence of signal. For each couple $\{\mu,\mathrm{SNR}\}$, modal parameters were estimated 50 times. For each mode of the synthetic signal, the uncertainty in frequency or damping is defined as the mean of the absolute values of the relative error between the original and the estimated data. These uncertainties, expressed in dB, are shown as contour plots in Fig. 4.

It can be seen in Fig. 4 that the uncertainties are very small for both dampings and frequencies even for high modal overlaps and low SNR. In general, the uncertainty increases with μ and decreases slightly when SNR increases. The HRMA gives better estimations of the eigenfrequencies and dampings than the FFT for a wide range of μ and SNR. Since the modal overlap μ generally increases in the impulse response of a plate, and the SNR decreases with the frequency, the HRMA gives access to significantly more modes than the usual FT-based modal-analysis techniques and is thus of great interest in the present context.

5. Optimisation procedure

This section describes how to derive, in two steps, the complex moduli of elasticity of the homogenised equivalent material of the sandwich plate $\{E_x^H,\eta_x^H,E_y^H,\eta_y^H,G_{xy}^H,\eta_{xy}^H,G_{xz}^H,\eta_{xz}^H,G_{yz}^H,\eta_{yz}^H,\nu_{xy}^H,\eta_\nu^H\}$ from the experimental and numerical values of the modal frequencies and dampings f_n^{XP}, f_n^{Num}, α_n^{XP}, and α_n^{Num}.

5.1. Elastic properties

The estimation of the elasticity parameters $\{E_x^H,E_y^H,G_{xy}^H,G_{xz}^H,G_{yz}^H,\nu_{xy}^H\}$ is done by comparing the experimental and numerical modal frequencies. The estimation problem to solve is nonlinear and several orders of magnitude are involved in the property values. The following cost-function was used:

$$C_f=\sum_{n=1}^{N}\left(\frac{f_n^{\mathrm{XP}}-f_n^{\mathrm{Num}}}{f_n^{\mathrm{XP}}}\right)^2 \tag{20}$$

A steepest-descent (with backtracking) algorithm [62] using rigidities $\{D_1,D_2,D_3,D_4,D_5,D_6\}$ as design variables has been chosen. In the present case, the coefficients of the gradient can be easily derived analytically, making the method easy to implement and computationally light.

Estimation results obtained by gradient methods are known to be very dependent on the initial values of the parameters. To minimise the influence of the starting point, the following initialisation strategy for the rigidities has been chosen:

1. Initial values of in-plane rigidities D_1, D_2, D_3 and D_6 are the most influential; they were derived from the three lowest modal frequencies of the panel, as proposed in [22].
2. Initial values of out-of-plane rigidities D_4 and D_5 are less critical; homogenisation theory proposed by Gibson [63] for honeycomb core sandwich panels is used. This theory requires a value for the elasticity moduli of the material composing the honeycomb core. The first estimation was based on static tests.

In the following examples, 10 iterations were enough to reach convergence: 10^{-7} for the gradient.

5.2. Damping properties

As can be seen in Eq. (17), modal dampings depend linearly on the loss factors $\{\eta_x^H,\eta_y^H,\eta_{xy}^H,\eta_{xz}^H,\eta_{yz}^H,\eta_\nu^H\}$ once the rigidities have been found. The estimation of the loss factors is therefore much easier than that of the elasticity parameters. A simple least-square optimisation procedure is sufficient to estimate the loss factors from the modal dampings.

The following cost-function has been chosen:

$$C_\alpha=\sum_{n=1}^{N}\left(\frac{\alpha_n^{\mathrm{XP}}-\alpha_n^{\mathrm{Num}}}{\alpha_n^{\mathrm{XP}}}\right)^2 \tag{21}$$

The optimisation procedure is not iterative and needs no particular initialisation.

5.3. Determination of the order Q of the polynomial basis and of the number N of included modal parameters

Two parameters have to be chosen in order to apply the optimisation procedures described in Sections 5.1 and 5.2. These methodological parameters are the order Q of the polynomial basis associated with the extended Rayleigh–Ritz procedure (see Section 3.2) and the number N of modal parameters (frequencies or dampings) to be included in the optimisation procedure.

The parameters Q and N can be chosen differently for the estimation of the elastic material properties and for the estimation of the material loss factors respectively. For the estimation of the elastic material properties, the parameters Q_f

and N_f that minimise the cost functions C_f given by Eq. (20) are chosen. For the estimation of the damping properties, the parameters Q_α and N_α that minimise the cost functions C_α given by Eq. (21) are chosen. Selecting the optimal Q and N values is done empirically by running the optimisations for different values of these parameters, typically in the ranges $N \in \{20,40\}$ and $Q \in \{10,18\}$.

5.4. Sensitivity analysis

For the estimation procedures described in Sections 5.1 and 5.2 to be efficient, modal frequencies and dampings must convey a sufficient amount of information relative to each parameter to be estimated. In other words, modal dampings and frequencies have to be sensitive to the parameters of interest.

Relevant sensitivities can be defined and calculated analytically. The sensitivity of the modal value τ to the parameter γ is noted S_γ^τ and defined by Eq. (22): if γ is increased by 1 percent, τ increases by S_γ^τ percent.

$$S_\gamma^\tau = \frac{\Delta\tau}{\Delta\gamma}\frac{\gamma}{\tau} = \frac{\dfrac{\Delta\tau}{\tau}}{\dfrac{\Delta\gamma}{\gamma}} \tag{22}$$

According to Eq. (16) and with the same notations, the sensitivity $\mathcal{S}_{D_k}^{f_n}$ of the nth modal frequency f_n to the rigidity $D_k \in \{D_1,D_2,D_3,D_4,D_5,D_6\}$ can be written as

$$\mathcal{S}_{D_k}^{f_n} = \frac{D_k u_{nk}}{8\pi^2 f_n^2 t_n} \tag{23}$$

Similarly, using Eq. (17), the sensitivity $\mathcal{S}_{\eta_k}^{\alpha_n}$ of the nth modal damping α_n to the loss factor $\eta_k \in \{\eta_1,\eta_2,\eta_3,\eta_4,\eta_5,\eta_6\}$ can be written as

$$\mathcal{S}_{\eta_k}^{\alpha_n} = \frac{\eta_k D_k u_{nk}}{4\pi f_n \alpha_n t_n} \tag{24}$$

The amount of information relative to one given parameter and contained in one given mode can be easily quantified with Eqs. (23) and (24). Examples are given in Figs. 7, 10 and 12 (see Section 7).

6. Validation of the estimation procedure

A validation of the mechanical model and procedures given in Sections 2, 3 and 5 is proposed as follows: the experimental results of the modal analysis are replaced by those of the simulation of a finite-element model (FEM) of two virtual plates with known properties. The modes of a homogeneous thick-plate as modelled using the FEM are first compared to those given by the extended Rayleigh–Ritz procedure applied to the mechanical model given in Section 2. The method for deriving elasticity and damping parameters as sketched in Fig. 1 is afterwards validated on a virtual sandwich plate.

Table 1
Geometry and constituent densities of the homogeneous virtual plate (HVP) and of the virtual sandwich-plate (VSP).

	l_x (m)	l_y (m)	h (m)		ρ (kg/m^3)	
HVP	0.4	0.6	4×10^{-3}		700	
			Core	Skin	Core	Skin
VSP	0.4	0.6	4×10^{-3}	0.2×10^{-3}	40	700

Table 2
Mechanical parameters chosen for the homogeneous virtual plate (HVP) and for the virtual sandwich-plate (VSP).

	$\underline{E}_x$	$\underline{E}_y$	$\underline{\nu}_{xy}$	$\underline{G}_{xy}$	$\underline{G}_{xz}$	$\underline{G}_{yz}$
HVP						
Real part	4 GPa	5 GPa	0.33	1 GPa	10^{-2} GPa	10^{-2} GPa
Loss factor (%)	2	5	1	0.5	1	1
VSP skins						
Real part	4 GPa	5 GPa	0.33	1 GPa	1 GPa	1 GPa
Loss factor (%)	2	5	1	0.5	1	1
VSP core						
Real part	1×10^{-3} GPa	1×10^{-3} GPa	0.33	1×10^{-3} GPa	1×10^{-2} GPa	3×10^{-2} GPa
Loss factor (%)	1	1	1	1	3	5

6.1. Finite-element model of the virtual plates

To validate the extended Rayleigh–Ritz procedure applied to the mechanical model, a homogeneous thick virtual plate was designed. A FE-model of the sandwich panel has also been built to test the accuracy of the estimation method. The chosen sandwich plate is made of three homogeneous layers and is symmetrical with respect to its mid-plane. Geometrical, mechanical and mass parameters of the two plates are given in Tables 1 and 2.

For the two virtual plates under study, the finite-element model is built on a 2D rectangular mesh made of 60 by 60 regularly spaced points. This value is justified at the end of this section. At each point an 8-node shell element is placed with a linear expansion of the in-plane displacements in the thickness coordinate and a constant transverse displacement through the thickness (COQ8 of the Cast3M code [64]). Each of these elements possess 6 degrees of freedom (the translations in the x-, y-, and z-directions and the rotations around the x-, y- and z-axes). In the case of the virtual sandwich plate, the three-layers are modelled as one equivalent layer as in Section 2.3.

6.2. Modal frequencies and dampings of the virtual plates

Finite-element modelling and the associated computations have been performed using Cast3M [64], a free software developed by the French Centre for Atomic Energy (CEA). This software is used here as it allows to find the complex modes (modal shapes ξ_n^{FEM}, dampings α_n^{FEM} and frequencies f_n^{FEM}) of a problem put in the form: $\boldsymbol{K}+\mathrm{j}\omega\boldsymbol{C}-\omega^2\boldsymbol{M}=\boldsymbol{0}$. In this formulation, $\boldsymbol{M}$, $\boldsymbol{C}$ and $\boldsymbol{K}$ must be real matrices to be accepted by the VIBC function of the Cast3M code. Complex modes are then found by solving a complex valued generalised eigenvalue problem using a QZ-algorithm. According to the possibilities offered by Cast3M, modal frequencies and dampings of the virtual plates are computed using the following procedure:

1. The conservative system is described according to the constitutive model of Section 2.2 with no hysteretic damping taken into account. A mass matrix $\boldsymbol{M}$ and a real stiffness matrix $\boldsymbol{K}'$ are deduced from this model.
2. The N first modal frequencies $\{f_n^{\mathrm{FEM}}\}_{n\in[1,N]}$ of the conservative system are computed by solving, in the Fourier domain, the real-valued eigenvalue problem $\boldsymbol{K}'-\omega^2\boldsymbol{M}=0$.
3. The non-conservative system is described according to the constitutive model of Section 2.2, including hysteretic damping. A mass matrix $\boldsymbol{M}$ and a complex stiffness matrix $\boldsymbol{K}=\boldsymbol{K}'+\mathrm{j}\boldsymbol{K}''$ are deduced from this model.
4. The "light damping hypothesis," is retained. The real part of the modal frequencies of the non-conservative system are thus already known (see Section 3.1).
5. For each one of the N first modes of the non-conservative system, the following operations are then performed:
   (a) The dynamic equation of the dissipative system are formulated, in the Fourier domain, as $-\omega^2\boldsymbol{M}\boldsymbol{q}+\mathrm{j}\omega\boldsymbol{C}\boldsymbol{q}+\boldsymbol{K}'\boldsymbol{q}=\boldsymbol{0}$ with $\boldsymbol{C}=\boldsymbol{K}'/(2\,\pi\,f_n^{\mathrm{FEM}})$. The problem is thus formulated as expected by the VIBC function with $\boldsymbol{C}$ real but frequency-dependent. Its important to notice that this equation models correctly the hysteretic damping model described in Section 2.2 only near $\omega\simeq 2\pi f_n^{\mathrm{FEM}}$.
   (b) The modal loss factor α_n is obtained as the imaginary part of the eigenvalue of this new problem solved near $\omega\simeq 2\pi f_n^{\mathrm{FEM}}$.

For the homogeneous virtual plate, increasing the number of elements above 60 elements per side results in less than a 1 percent relative variation of the 35 first modal frequencies (conservative and non-conservative cases) and in less than 0.4 percent of the 35 first modal dampings. The same convergence is observed for the 3-layer virtual sandwich plate. Thus, 60 elements per side are enough to ensure the desired precision on the analysis of the first 35 modes of the two plates.

6.3. Validation of the extended Rayleigh–Ritz resolution of the mechanical model

Comparing the modal frequencies and dampings given by the extended Rayleigh–Ritz resolution method (18-order) and by the FE-model for the homogeneous thick virtual plate provides an estimate of the reliability of the retained mechanical model coupled with the extended Rayleigh–Ritz resolution method for the first 35 modes.

The plate under study in the present section is not a sandwich panel as the one modelled in Section 2 but a homogeneous thick plate. For such homogeneous plates, values for the shear correction factors are usually chosen between 2/3 and 5/6 instead of 1, which is recommended only for sandwich panels [50]. Values of $\kappa_{yz}=\kappa_{xz}=0.7$ have been arbitrarily chosen here in the range [0.666,0.833].

With shear correction factors $\kappa_{yz}=\kappa_{xz}=0.7$, the mean absolute difference between FE-results and Rayleigh–Ritz results is lower than 1.2 percent for modal frequencies and lower than 25 percent for modal dampings. The larger error on modal dampings may be explained as follows. The damping matrix $\boldsymbol{C}$ provided to the FEM results from the writing of the stiffness matrix and is not necessarily diagonal when expressed in the basis of the conservative modes. By contrast, the extended Rayleigh–Ritz procedure accounts for dissipation by associating one damping coefficient α_n^{Num} to each mode, neglecting by construction any coupling between conservative modes.

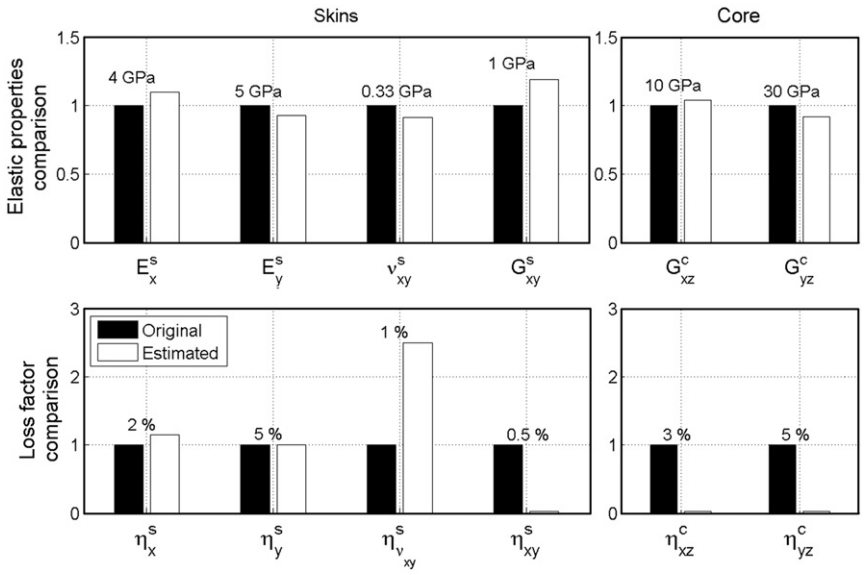

Fig. 5. Comparison between the values of the mechanical parameters used in the FEM (Original), and their estimated values (Estimated) for each constituent (skins, core) of the virtual sandwich plate. Original parameters are represented as black bars with their numerical value indicated above. White bars represent the ratio of the estimated to the original parameters. Elasticity parameters have been estimated with 35 modes and with a model order $Q=16$. Loss-factors have been estimated with 28 modes and with a model order $Q=18$.

6.4. Estimation results for the 3-layer virtual sandwich-plate

A 3-layer virtual sandwich-plate has been used to validate the estimation procedure described in Fig. 1. Since, for this 3-layer virtual sandwich-plate, convergence problems were encountered with the steepest-descent algorithm, a simplex search method [65] was used instead in this case (function *"fminsearch"* in Matlab™). The initialisation procedure remains the same as the one described in Section 5.1. For all other optimisations, the steepest-descent algorithm is used.

Based on the first $N=35$ modal frequencies given by the FEM and using a Rayleigh–Ritz order $Q=16$, the estimated values of the elasticity parameters are compared to the original values given to the FEM. The loss factors have been estimated with $N=28$ modes and a model order $Q=18$. The estimated mechanical parameters are presented in Fig. 5 for each layer of the sandwich.

The residual mismatch between the results of estimation and the original values is discussed here. The mean absolute value $\langle |\Delta f_n/f_n| \rangle$ of the relative difference between experimental and numerical modal frequencies is 2.6 percent. For the dampings, the residual mismatch $\langle |\Delta \alpha_n/\alpha_n| \rangle$ is 21.6 percent. These orders of magnitude, as compared to the one obtained in Section 6.3, suggest that the assumption that a 3-layer sandwich plate can be modelled as a simple homogeneous thick-plate is correct in the frequency range under study.

It can be seen in Fig. 5 that the agreement between estimated and original parameters is globally very good. In-plane elasticity parameters of the skins and out-of-plane elasticity parameters of the core are estimated with a mean absolute relative error of 10.2 percent. Principal in-plane loss-factors η_x^s and η_y^s are estimated with a comparable accuracy of 7.5 percent. The imaginary part of $\underline{\nu}_{xy}^s$ is largely overestimated while the imaginary part of $\underline{G}_{xy}^s$ is underestimated. However, the overestimation of one parameter may be the result of the underestimation of the other, by compensation. The imaginary parts of $\underline{G}_{xz}^c$ and $\underline{G}_{yz}^c$ are assigned zero values by the estimation process. The fact that zero values are found illustrates the limitations of the thick-plate model under Reissner–Minldin hypothesis. Physically, this underestimation is due to the fact that only a marginal part of the total energy-loss per cycle is dissipated through the mechanical couplings described by $\underline{G}_{xz}^c$ and $\underline{G}_{yz}^c$. Modal damping factors are thus here not very sensitive to these material loss factors.

A complete validation study should have established the validity limits of the estimation method. Even though this is not what has been done here, the above results suggest that the mixed numerical/experimental procedure is potentially an accurate tool for the estimation of the main elasticity moduli and loss-factors of 3-layer sandwich plates.

7. Experimental results

7.1. Plate specimens

Three different sandwich panels with heterogeneous cores have been investigated. The first two – HC_1 and HC_2 – are rectangular lightweight honeycomb sandwich panels. Their skins and honeycomb cores are made of epoxy and paper. The third panel, made of two stainless steel sheets (skins) and two bidirectionally corrugated steel layers with a 20 percent

Table 3
Geometry and constituent-densities of three sandwich panels HC_1, HC_2, and CC. The characteristic side-length of the core-cells is s_{cell}.

	l_x (cm)	l_y (cm)	h^s (mm)	h^c (mm)	s_{cell} (mm)	ρ^c (kg/m^3)	ρ^s (kg/m^3)
HC_1	39.15	59.10	0.20	4.88	4.0	37.8	713
HC_2	80.00	99.95	0.20	3.80	4.0	37.8	713
CC	17.78	22.86	0.20	1.48	1.0	2164	7800

Table 4
Estimated mechanical parameters for panel HC_1. Parameters relative to the skins and the core are obtained after inversion of Eqs. (3) and (4).

	$\underline{E}_x$	$\underline{E}_y$	$\underline{\nu}_{xy}$	$\underline{G}_{xy}$	$\underline{G}_{xz}$	$\underline{G}_{yz}$
Equivalent plate						
Real part	1.0 GPa	1.4 GPa	0.25	0.46 GPa	12 MPa	26 MPa
Loss factor (%)	1.5	1.3	0	1.2	5.5	4.1
Core						
Real part	–	–	–	–	12 MPa	26 MPa
Loss factor (%)	–	–	–	–	5.5	4.1
Skins						
Real part	4.8 GPa	6.8 GPa	0.25	5.6 GPa	–	–
Loss factor (%)	1.5	1.3	0	1.2	–	–
Skins						
Tensile tests	5.3 GPa $\pm$0.5 GPa	7.3 GPa $\pm$0.7 GPa	0.28 $\pm$ 0.04	–	–	–

relative density (core), is denoted CC (for "corrugated core"). The geometry and mass parameters of each panel are given in Table 3.

The $E^s_{x,y}/G^c_{yz,xz} \simeq 100$ criterium (see Section 2.1) that must be satisfied turns out to be met for all the plates that have been tested. According to Section 1, the sandwich core can be considered as homogeneous in the in-plane directions up to a given frequency f_{max} if the corresponding wavelength λ^{min} contains at least 50 cells [39]. For a typical cell side-length s_{cell} and height h, this implies that $\lambda^{min}/s_{cell} > 50$. Moreover, plates must be thick-enough in order that out-of-plane elasticity parameters and loss-factors be estimated, but not too thick for the thick-plate theory to remain valid. This implies $2h/\lambda^{min} < 0.08$ [42]. The validity of these assumptions will be discussed.

7.2. Results for panel HC_1

Panel HC_1 was acoustically excited [27] and 46 modes were identified. Elasticity parameters and loss-factors were estimated with $N=40$ modes and a model order $Q=14$ using the steepest-descent algorithm of Section 5.1. The estimated parameters of the equivalent homogeneous plate and the corresponding skin and core parameters are given in Table 4.

The equivalent plate corresponding to panel HC_1 was found to be slightly orthotropic. This is a consequence of the laminated skins and of the orthotropy of the honeycomb structure. One can also notice that very low values are found for the loss factors associated with the Poisson ratio: little energy is dissipated via the Poisson effect in panel HC_1. Also, out-of-plane loss factors are relatively larger than the in-plane loss factors; this denotes that dissipation in honeycomb core structures is larger for out-of-plane shearing than for bending.

Static tensile tests have been performed on two samples of the skin material in the x- and y-directions respectively. The results are: $E^s_x = 5.3 \pm 0.5$ GPa, $\nu^s_{xy} = 0.28 \pm 0.04$, $E^s_y = 7.3 \pm 0.7$ GPa, $\nu^s_{yx} = 0.27 \pm 0.04$. These values are in excellent agreement with the values estimated using the proposed method. This constitutes an additional validation for the proposed method.

The optimisation procedure consists in minimising the difference between the experimental modal frequencies and dampings and numerical modal frequencies and dampings. The residual differences are presented in Fig. 6 and provide an estimation of the reliability of the method. One can observe that there is a very low relative difference between the measured and numerical modal frequencies: $\langle |\Delta f_n/f_n| \rangle = 2$ percent. Thus, the homogeneous thick-plate model based on the Reissner–Mindlin hypothesis agrees with the real dynamical behavior of panel HC_1. Moreover, there is also a low relative difference between measured and numerical modal dampings: $\langle |\Delta \alpha_n/\alpha_n| \rangle = 10$ percent. The frequency-independent loss factors combined with the "light damping" hypothesis appears to be a good model for the constitutive material of panel HC_1.

Based on the estimated values given in Table 4, the modal shapes can be computed by means of the extended Rayleigh–Ritz procedure. In the y-direction, panel HC_1 has a maximum of eight nodal lines in the frequency range under consideration. This corresponds to $4.5\lambda^{min}$: the shortest wavelength is 13 cm and contains $\lambda^{min}_y/s_{cell} \simeq 30$ cells. In the x-direction, there are up to six nodal lines: $\lambda^{min}_x = 11$ cm, $\lambda^{min}_x/s_{cell} \simeq 28$ cells. Theoretically, this is hardly sufficient for the

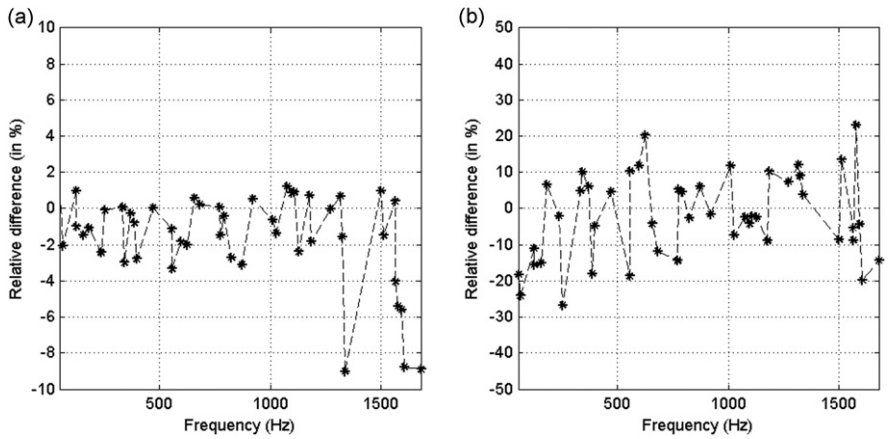

Fig. 6. Residual differences on eigenfrequencies (a) and dampings (b) for panel HC_1. Numerical values have been obtained using elasticity and damping parameters from Table 4.

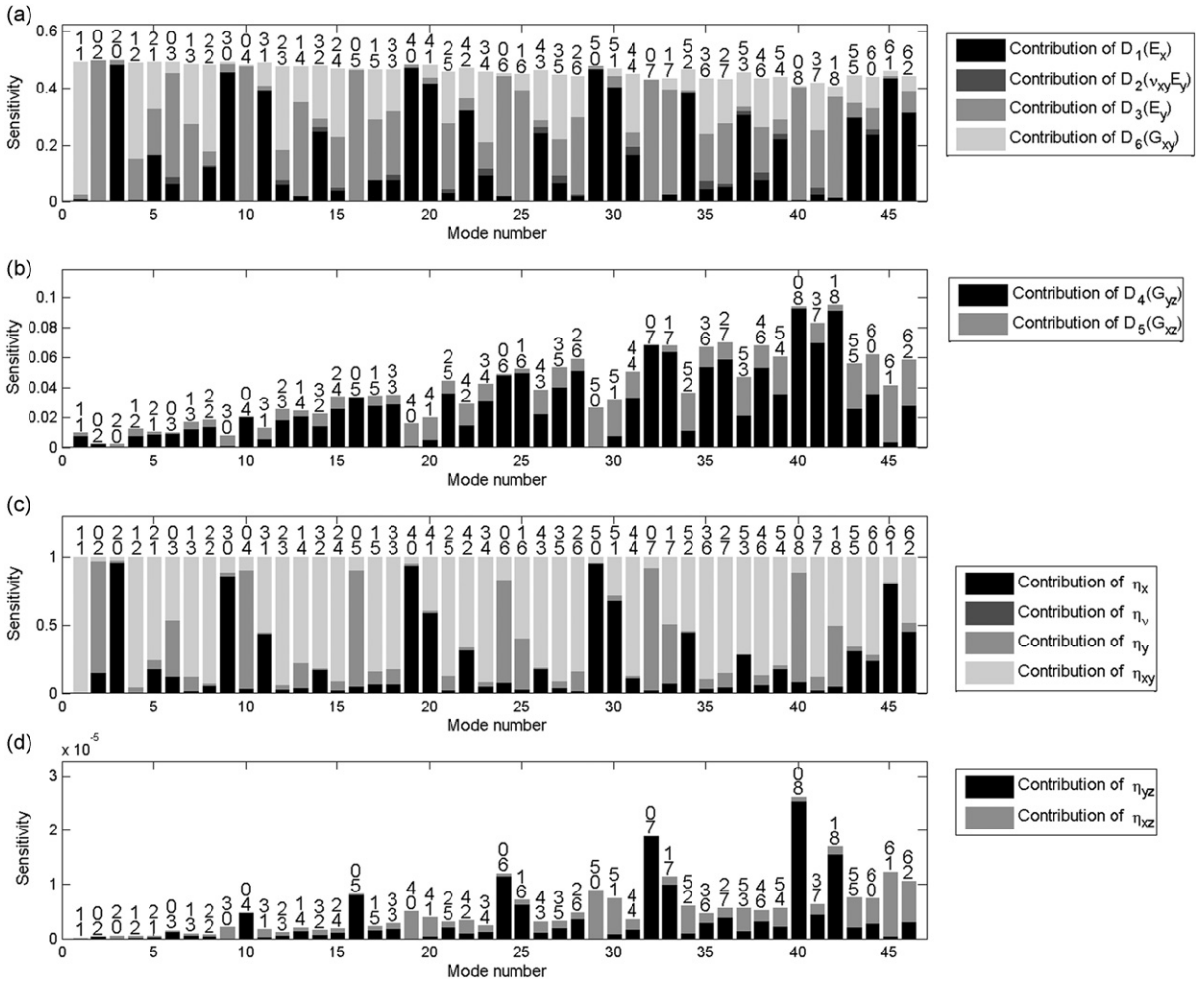

Fig. 7. Sensitivities of the modal frequencies to the in-plane (a) and the out-of-plane (b) elasticity parameters. Sensitivities of the modal dampings to the in-plane (c) and the out-of-plane (d) loss factors for panel HC_1. Modes are identified by the numbers of their nodal lines in the *x*- and *y*-directions (top and bottom numbers respectively, on top of each bar).

core to be considered as homogeneous. The condition $2h/\lambda^{\min} \leqslant 0.08$ is met for almost all modes since $2h/\lambda^{\min} = 0.08$ in the y-direction and $2h/\lambda^{\min} = 0.1$ in the y-direction. However, a very good agreement is observed in Fig. 6 between the homogeneous model and the experimental values. Therefore, 30 cells per wavelength may be enough in the present case for the core to be considered as homogeneous. The thick-plate theory also seems sufficient for $2h/\lambda^{\min} = 0.1$.

Sensitivities of the modal frequencies and dampings to the in-plane and out-of-plane mechanical parameters for panel HC_1 are shown in Fig. 7. Modal frequencies and dampings are sensitive to all the in-plane elasticity and damping parameters. The estimated in-plane mechanical properties are thus reliable. Sensitivities to the out-of-plane mechanical properties are relatively important. This ensure a high degree of confidence for the estimated values of $\mathrm{Re}(\underline{G}^H_{xz})$ and $\mathrm{Re}(\underline{G}^H_{yz})$ since a large number of sensitive modes are involved in the optimisation procedure. Sensitivity to the out-of-plane loss factors is one order of magnitude lower. Thus, estimated out-of-plane loss factors are less reliable than in-plane loss factors.

7.3. Results for panel HC_2

Panel HC_2 was excited by an impact hammer and 26 modes were extracted. Elasticity parameters and loss-factors were estimated with $N=26$ modes and a model order $Q=14$ using the steepest-descent algorithm of Section 5.1. The estimated parameters of the equivalent homogeneous plate are given in Table 5.

As can be seen in Fig. 8, in-plane and out-of plane elasticity and damping parameters are similar to those of panel HC_1. Theoretically, if the cores of the two plates were made of the same material (which is not known with certainty but seems to be the case), $\mathrm{Re}(\underline{G}^H_{xz})$ and $\mathrm{Re}(\underline{G}^H_{yz})$ should be equal for both panels, according to Eq. (3). This is verified here with a good

Table 5
Estimated mechanical parameters for panel HC_2. Parameters relative the skins and the core are obtained after inversion of Eqs. (3) and (4).

	$\underline{E}_x$	$\underline{E}_y$	$\underline{\nu}_{xy}$	$\underline{G}_{xy}$	$\underline{G}_{xz}$	$\underline{G}_{yz}$
Equivalent plate						
Real part	1.0 GPa	1.2 GPa	0.27	0.48 GPa	13 MPa	28 MPa
Loss factor (%)	1.0	1.1	0.0	3.2	44	30
Skins						
Real part	3.8 GPa	4.7 GPa	0.27	1.9 GPa	–	–
Loss factor (%)	1.0	1.1	0.0	1.2	–	–
Core						
Real part	–	–	–	–	13 MPa	28 MPa
Loss factor (%)	–	–	–	–	44	30

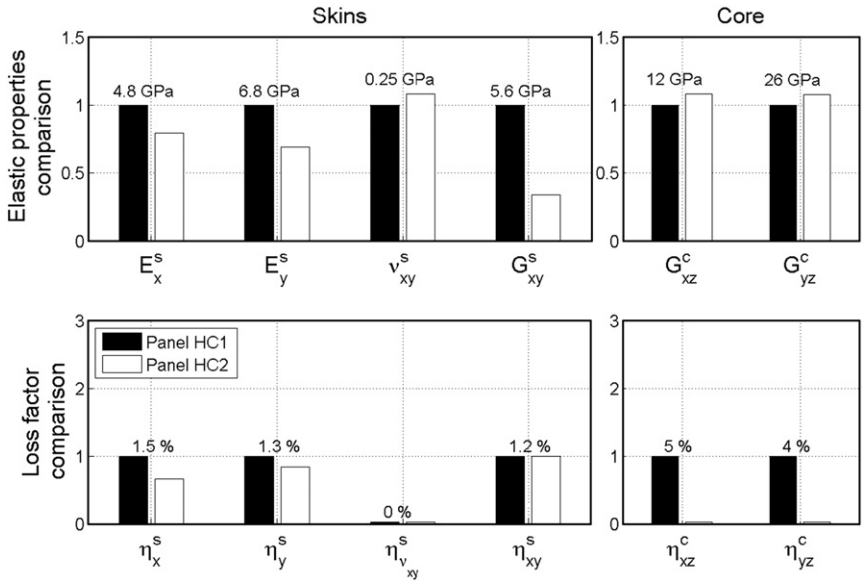

Fig. 8. Comparison between the skins and core mechanical parameters estimated from panels HC_1 and HC_2. Numerical values indicated as references black bars correspond to the results obtained for the panel HC_1. White bars represent the ratio of the estimated value for HC_2 relatively to the one estimated for HC_1.

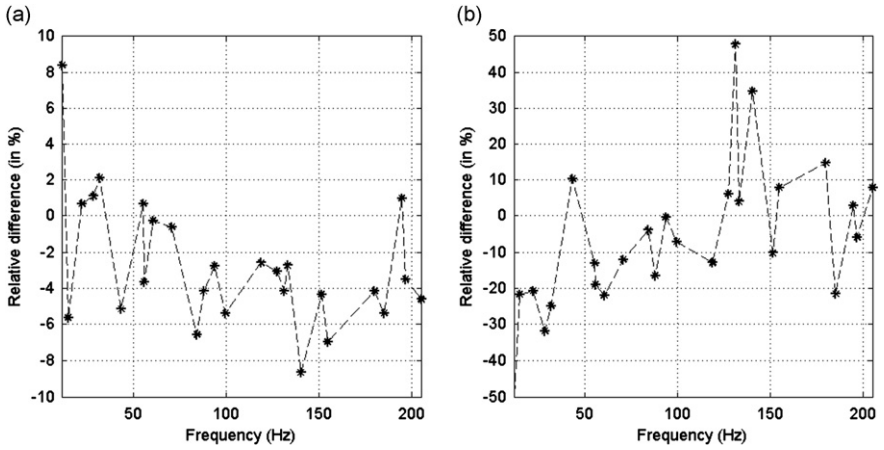

Fig. 9. Residual differences on eigenfrequencies (a) and dampings (b) for panel HC_2. Numerical values have been obtained with elasticity and damping parameters given in Table 5.

degree of precision. This robustness against the size of test-panels constitutes an additional indication that the proposed method is reliable with regard to material properties.

The residual differences $\langle |\Delta f_n/f_n| \rangle$ and $\langle |\Delta \alpha_n/\alpha_n| \rangle$ for panel HC_2 are shown in Fig. 9. They are approximately 3.8 percent and 16.7 percent respectively. Plate and material models can be considered as appropriate for these honeycomb core sandwich panels (panels HC_1 and HC_2).

Based on the estimated values given in Table 5, the modal shapes of the extracted modes can be computed with the extended Rayleigh–Ritz procedure (Section 3.2). In the y-direction, panel HC_2 has a maximum of five nodal lines in the frequency range under consideration: its side-length is $3\lambda_y^{\min}$ and $\lambda_y^{\min} = 33$ cm, containing $\simeq 80$ cells. In the x-direction, panel HC_2 has a maximum of five nodal lines: $\lambda_x^{\min} = 26.5$ cm, $\lambda_x^{\min}/s_{\text{cell}} \simeq 65$ cells. This is more than sufficient for the core to be considered as homogeneous. Moreover in both directions, $2h/\lambda^{\min} \simeq 2.4 \times 10^{-2} < 0.08$, which is theoretically sufficient for modal frequencies to be predicted using thick-plate theory. The core of panel HC_2 can be considered as homogeneous and all the modal frequencies can be predicted using thick-plate theory.

Sensitivities of the modal frequencies and dampings to the in-plane and out-of-plane mechanical parameters for panel HC_2 are shown in Fig. 10. Sensitivities to the elastic out-of-plane mechanical properties are lower for panel HC_2 than for panel HC_1. However, since results obtained on panel HC_2 are in close agreement with those obtained with panel HC_1, this suggests that a sensitivity of $\simeq 10^{-2}$ may still yield reliable results. Very low sensitivities to the out-of-plane loss factors explain that values of loss factors estimated on panel HC_2 deviate significantly from the values obtained with panel HC_1.

7.4. Results for panel CC

Panel CC was excited with an impact hammer. Elasticity material parameters have been estimated with $N=35$ modes and a model order $Q=14$ using the steepest-descent algorithm of Section 5.1. Loss factors have been estimated with $N=23$ modes and a model order $Q=13$. The estimated parameters of the equivalent homogeneous plate are given in Table 6.

At first, it can been seen from Table 6 that the real parts of $\underline{E}_x$ and $\underline{E}_y$ for skins match standard values for the elasticity modulus of steel ($\simeq 210$ GPa [49]). Since panel CC is a metallic sandwich panel, its loss factors are much lower than those of panels HC_1 and HC_2. The residual differences on eigenfrequencies and dampings are shown in Fig. 11. It can be seen that the uncertainty on the estimation of damping is large $\langle |\Delta \alpha_n/\alpha_n| \rangle = 34$ percent and increases with frequency. Since the estimated structural loss factors are very low, the measured modal dampings are very sensitive to the way the panel is suspended (thin wires) and to damping due to acoustical radiation. Moreover, these damping mechanisms are also mode-dependant. In the high-frequency range, a systematic discrepancy appears between the measured and the (numerically) modelled damping factors. For the equivalent homogeneous plate, the coincidence frequency f_c is estimated to be approximately 4 kHz. Damping due to acoustical radiation increases as the modal frequency comes close to f_c. In the same spirit, the difference between f_n^{XP} and f_n^{Num} seems to be systematically negative by $\simeq 2$ percent. By order of magnitude, this is consistent with air loading in the low-frequency range. The relative differences between experimental and numerical modal frequencies remain small $\langle |\Delta f_n/f_n| \rangle = 2.3$ percent.

Based on the estimated values given in Table 6, the modal shapes of the extracted modes can be computed by means of the extended Rayleigh–Ritz procedure of Section 3.2. In the y-direction, panel CC has a maximum of seven nodal lines in the studied frequency range: its side-length is $4\lambda_y^{\min}$ and $\lambda_y^{\min} = 5.7$ cm, containing $\lambda_y^{\min}/s_{\text{cell}} \simeq 55$ cells. In the x-direction, panel CC has a maximum of six nodal lines: $\lambda_x^{\min} = 5$ cm, containing $\lambda_x^{\min}/s_{\text{cell}} \simeq 50$ cells. This is sufficient for the core to be considered as homogeneous. Also, $2h/\lambda^{\min} = 6.6 \times 10^{-2} < 0.08$ in the y-direction, and $2h/\lambda^{\min} = 7.52 \times 10^{-2} < 0.08$ in the y-direction, which is also sufficient for modal frequencies to be predicted by the thick-plate theory. In the frequency range

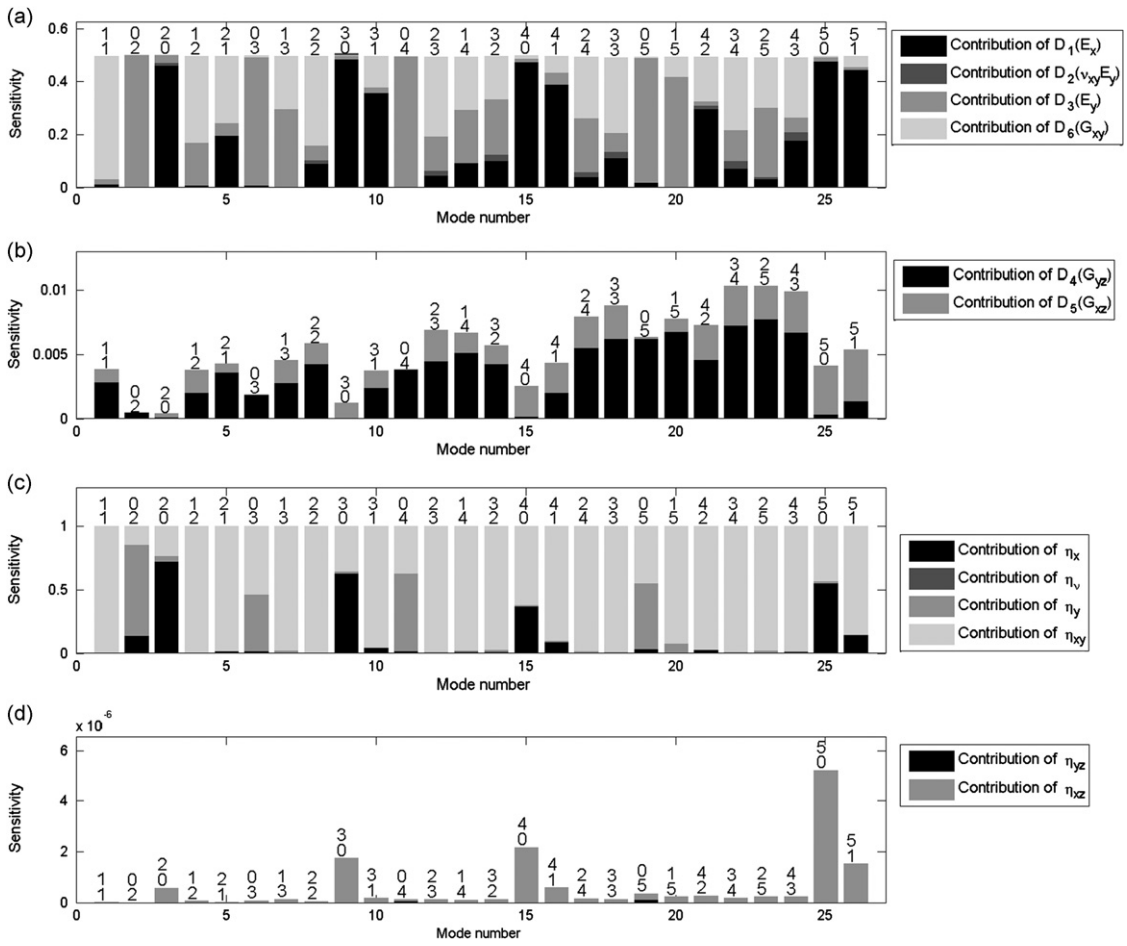

Fig. 10. Sensitivities of the modal frequencies to the in-plane (a) and out-of-plane (b) elasticity parameters. Sensitivities of the modal dampings to the in-plane (c) and out-of-plane (d) loss factors for panel HC_2. Modes are identified by the numbers of their nodal lines in the *x*- and *y*-directions (top and bottom numbers respectively, on top of each bar).

Table 6
Estimated mechanical parameters for panel CC. Parameters relative the skins and the core are obtained after inversion of Eqs. (3) and (4).

	$\underline{E}_x$	$\underline{E}_y$	$\underline{\nu}_{xy}$	$\underline{G}_{xy}$	$\underline{G}_{xz}$	$\underline{G}_{yz}$
Equivalent plate						
Real part	117 GPa	102 GPa	0.33	43 GPa	77 GPa	163 GPa
Loss factor (%)	0.1	0.1	0.0	0.1	0.0	0.7
Skins						
Real part	229 GPa	200 GPa	0.33	84 GPa	–	–
Loss factor (%)	0.1	0.1	0.0	0.1	–	–
Core						
Real part	–	–	–	–	77 GPa	163 GPa
Loss factor (%)	–	–	–	–	0.0	0.7

under consideration, the core of panel CC can be considered as homogeneous and the high modal frequencies are expected to be well predicted by the thick-plate theory.

Results of the sensitivity analysis are presented in Fig. 12 for panel CC. It can be seen that sensitivities to the out-of-plane properties are very low compared to sensitivities relative to the in-plane properties and also as compared to sensitivities to the out-of-plane properties of panels HC_1 and HC_2. This means that the modal frequencies and modal dampings are hardly influenced by the out-of-plane complex moduli. As a consequence, the estimations of these parameters must be interpreted very carefully. In this case the core material is too stiff (the last hypothesis listed in Section 2.1 is not valid): the out-of-plane shear moduli are too high to allow for their precise identification.

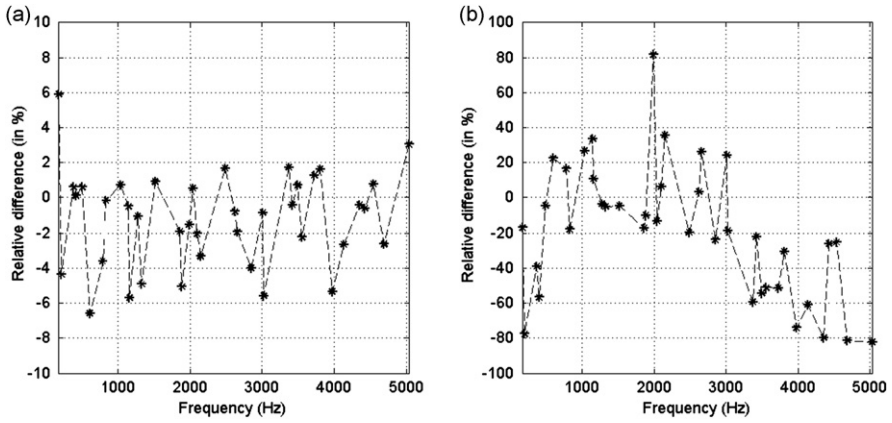

Fig. 11. Residual difference on eigenfrequencies (a) and dampings (b) for panel CC. Numerical values have been obtained using elasticity and damping parameters given in Table 6.

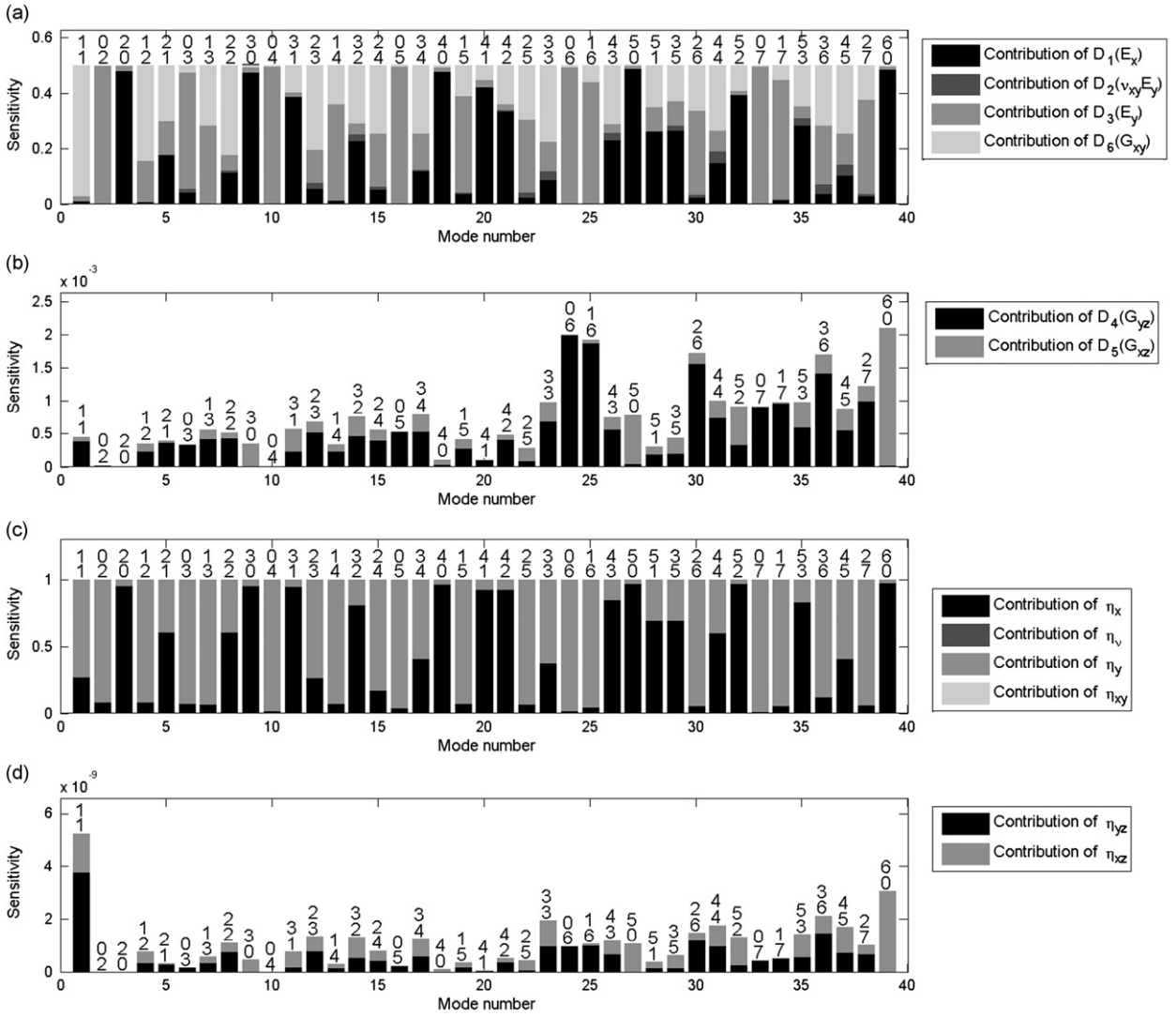

Fig. 12. Sensitivities of the modal frequencies to the in-plane (a) and out-of-plane (b) elasticity parameters. Sensitivities of the modal dampings to the in-plane (c) and out-of-plane (d) loss factors for panel CC. Modes are identified by the numbers of their nodal lines in the *x*- and *y*-directions (top and bottom numbers respectively, on top of each bar).

8. Conclusion

In this paper, a method for the measurement of six elasticity moduli and six loss-factors of the constituents of a three-layer symmetrical sandwich material, namely $\underline{E}^s_x$, $\underline{E}^s_y$, $\underline{\nu}^s_{xy}$, $\underline{G}^s_{xy}$, $\underline{G}^c_{xz}$, $\underline{G}^c_{yz}$, has been presented (sandwich structure in the *xy*-plane). The method directly extends the work of de Visscher et al. [23] by proposing a means to measure also *out-of-plane* complex moduli. It continues the work of Bastos et al. [33] with the inclusion of loss factors in the mixed experimental/numerical procedure. Compared to the work of Pagnacco et al. [26] and to that of Matter et al. [27,36], the present method does not require full-field measurements and is thus much simpler to implement and faster to execute. Compared to the method of [29,37,66], high resolution modal analysis allows for more modal data to be extracted and used for the estimation of the elastic and damping properties of sandwich materials. Moreover, residuals obtained in the present paper for modal frequencies ($\simeq 1$ percent) and dampings ($\simeq 10$ percent) are fully in agreement with residuals obtained in [36–38] which estimate mechanical parameters of sandwich panels using much less modal data than does the present study.

The method is suited to sandwich structures with heterogeneous cores (*e.g.* honeycomb cores) provided that the panels on which the tests are performed satisfy several geometrical requirements. It has been validated successfully on virtual plates. Results obtained on three sandwich panels suggest that the dynamic behaviour of the sandwich material can be accurately modelled using (1) an equivalent homogeneous plate modelled with first order shear deformation theory, (2) a simple hysteretic model of the type "$E(1+j\eta)$" for each constituent material and (3) the "light damping" hypothesis for the panel. The consistency of the results with those obtained by static measurements, or on two different panels having the same sandwich structure, also contributes to the validation of the method. The extensive sensitivity analysis combined with the examination of the residual differences left by the optimisation process yields the degree of confidence that can be attributed to the value of each extracted mechanical parameter.

Since this method is simple and needs no heavy experimental apparatus, it is suited to the in-line control of the production of sandwich-materials. This method can also replace classical tensile tests (with some profit) and also, within the frame of the proposed model, the dynamical mechanical analysis (DMA) for the measurement of elastic and damping material properties.

Acknowledgements

Authors would like to thank Étienne Corteel, Camille Besse, and Dirk Mohr for providing the different test samples that have been characterised in this paper. The authors also thank Kerem Ege for his support regarding high resolution modal analysis, Vincent de Greef for the tensile tests and, Brian F.G. Katz for English corrections.

Appendix A. Generation of the orthonormal polynomial basis

The orthonormal polynomial basis $\{p_i(\kappa)\}_{i\in[0,N]}$ [55,56] used in the extended Rayleigh–Ritz procedure of Section 3 is generated by an iterative Gram–Schmidt process as follows:

$$\begin{cases} i=0, & \tilde{p_0}(\kappa)=\frac{1}{\sqrt{2}} \\ i=1, & \tilde{p}_1(\kappa)=(\kappa-\langle \kappa p_0(\kappa),p_0(\kappa)\rangle)p_0(\kappa) \\ i>1, & \tilde{p}_i(\kappa)=(\kappa-\langle \kappa p_{i-1}(\kappa),p_{i-1}(\kappa)\rangle)p_{i-1}(\kappa)-\langle \kappa p_{i-2}(\kappa),p_{i-2}(\kappa)\rangle p_{i-2}(\kappa) \end{cases} \tag{A.1}$$

The scalar product between two polynomials $a(\kappa)$ and $b(\kappa)$ is: $\langle a(\kappa),b(\kappa)\rangle = \int_{-1}^{1} a(\kappa)b(\kappa)\,d\kappa$. The normalised and not-normalised versions of the ith element of the polynomial basis are denoted respectively by $p_i(\kappa)$ and $\tilde{p}_i(\kappa)$. The former is derived from the latter by: $\tilde{p}_i(\kappa)=\sqrt{\langle \tilde{p}_i(\kappa),\tilde{p}_i(\kappa)\rangle}\,p_i(\kappa)$. The basis is orthonormal since the following equation is satisfied: $\forall(i,j)\in[0,N]^2\ \langle p_i(\kappa),p_j(\kappa)\rangle=\delta_{ij}$, where δ_{ij} is the Kronecker symbol.

Appendix B. Analytical expressions of the derivatives of *T* and *U*

The matrices $\boldsymbol{K}$ and $\boldsymbol{M}$ of the eigenvalue problem $[\boldsymbol{K}-4\pi^2 f^2\boldsymbol{M}]\boldsymbol{q}=0$ (Section 3.2) are derived from the analytical expressions of the derivatives of T and U relatively to the generalised displacements L_{ij},M_{ij},N_{ij}. Those are related to the "natural" displacements Φ_x, Φ_y, and w_0 by

$$\Phi_x(x,y)=\sum_{i,j}L_{ij}p_i(x)p_j(y),\quad \Phi_y(x,y)=\sum_{i,j}M_{ij}p_i(x)p_j(y),\quad w_0(x,y)=\sum_{i,j}N_{ij}p_i(x)p_j(y) \tag{B.1}$$

The derivatives of the kinetic energy $T=(\rho^H\omega^2/2)\iint_{(S)}[(h^3/12)(\Phi_x^2+\Phi_y^2)+hw_0^2]\,dx\,dy$ are

$$\begin{cases} \dfrac{\partial T}{\partial L_{ij}}=\dfrac{\rho^H l_x l_y h\omega^2}{4}L_{ij} \\ \dfrac{\partial T}{\partial M_{ij}}=\dfrac{\rho^H l_x l_y h\omega^2}{4}M_{ij} \\ \dfrac{\partial T}{\partial N_{ij}}=\dfrac{\rho^H l_x l_y h\omega^2}{4}N_{ij} \end{cases} \tag{B.2}$$

The simplicity of the formulas is due to the fact that no space derivatives appear in the expression of the kinetic energy and that all products $p_i p_j$ $(i \neq j)$ cancel out once integrated (orthogonality of the polynomials).

The derivatives of the potential energy U (given by Eq. (7)) are

$$\begin{cases} \dfrac{\partial U}{\partial L_{ij}} &= \displaystyle\sum_{k=0}^{N}\left[-\frac{l_x}{2}D_4 N_{ik} I(j,k)+\frac{l_x}{l_y}D_4 L_{ik} J(j,k)-\frac{l_y}{2}D_5 M_{kj} I(i,k)+\frac{l_y}{l_x}D_5 L_{kj} J(i,k)\right] \\ \dfrac{\partial U}{\partial M_{ij}} &= \dfrac{l_x l_y}{4}D_5 M_{ij}+\displaystyle\sum_{k=0}^{N}\left[\frac{l_y}{l_x}D_1 M_{kj} J(i,k)-\frac{l_y}{2}D_5 L_{kj} I(k,i)+\frac{l_x}{l_y}D_6 M_{ik} J(j,k)\right] \\ &\quad +\cdots\sum_{k,l}\left[\frac{D_2}{2}I(i,k)I(l,j)+D_6 I(k,i)I(j,l)\right]N_{kl} \\ \dfrac{\partial U}{\partial N_{ij}} &= \dfrac{l_x l_y}{4}D_4 N_{ij}+\displaystyle\sum_{k=0}^{N}\left[\frac{l_x}{l_y}D_3 N_{ik} J(k,j)-\frac{l_x}{2}D_4 L_{ik} I(k,j)+\frac{l_y}{l_x}D_6 N_{kj} J(k,i)\right] \\ &\quad +\cdots\sum_{k,l}\left[\frac{D_2}{2}I(k,i)I(j,l)+D_6 I(i,k)I(l,j)\right]M_{kl} \end{cases} \tag{B.3}$$

where $\sum_{k,l}$ stands for $\sum_{(k,l)\in[0,N]^2}$ and where the following integrals have been introduced:

$$I(i,j)=\left\langle \frac{\mathrm{d}p_i(\kappa)}{\mathrm{d}\kappa}, p_j(\kappa)\right\rangle = \int_{-1}^{1}\frac{\mathrm{d}p_i(\kappa)}{\mathrm{d}\kappa}p_j(\kappa)\,\mathrm{d}\kappa, \quad J(i,j)=\left\langle \frac{\mathrm{d}p_i(\kappa)}{\mathrm{d}\kappa}, \frac{\mathrm{d}p_j(\kappa)}{\mathrm{d}\kappa}\right\rangle = \int_{-1}^{1}\frac{\mathrm{d}p_i(\kappa)}{\mathrm{d}\kappa}\frac{\mathrm{d}p_j(\kappa)}{\mathrm{d}\kappa}\,\mathrm{d}\kappa \tag{B.4}$$

Appendix C. Analytical expressions of t_n and u_k^n

The explicit expression of the coefficients t_n and u_k^n, representing respectively the nth modal mass (for some normalised displacement) and the k-contribution to the nth modal stiffness, are necessary to compute the numerical modal dampings and the sensitivities of the modal frequencies and dampings to the rigidities and loss factors respectively, as explained in Sections 3.3 and 5.4. The coordinates of the nth modal shape are denoted by $\{L_{lm}^n, M_{lm}^n, N_{lm}^n\}$. The calculation is sketched in Section 3.3. The expression of t_n is

$$t_n=\frac{\rho^H l_x l_y h}{8}\sum_{l,m}\left[(L_{lm}^n)^2+\frac{h^2}{12}((M_{lm}^n)^2+(N_{lm}^n)^2)\right] \tag{C.1}$$

Table D1
Notations for the geometrical and mass parameters of the panels.

l_x (m)	Length of the x-side of the plate
l_y (m)	Length of the y-side of the plate
h^s (m)	Skin thickness
h^c (m)	Core thickness
$h=h^c+2h^s$ (m)	Sandwich panel thickness
ρ^s (kg m^{-3})	Skin mass density
ρ^c (kg m^{-3})	Core mass density
$\rho^H=1/h\times(h^c\rho^c+2h^s\rho^s)$ (kg m^{-3})	Equivalent homogeneous plate mass density
s_{cell} (m)	Characteristic side-length of the core-cells

Table D2
Notations for the complex mechanical parameters (elastic parameters and loss factors) of the panels ($\mathrm{j}^2=-1$).

	Core	Skin	Equivalent homogeneous plate
Young modulus in the x-direction	$\underline{E}_x^c=E_x^c(1+\mathrm{j}\eta_x^c)$	$\underline{E}_x^s=E_x^s(1+\mathrm{j}\eta_x^s)$	$\underline{E}_x^H=E_x^H(1+\mathrm{j}\eta_x^H)$
Young modulus in the y-direction	$\underline{E}_y^c=E_y^c(1+\mathrm{j}\eta_y^c)$	$\underline{E}_y^s=E_y^s(1+\mathrm{j}\eta_y^s)$	$\underline{E}_y^H=E_y^H(1+\mathrm{j}\eta_y^H)$
Young modulus in the z-direction	$\underline{E}_z^c=E_z^c(1+\mathrm{j}\eta_z^c)$	$\underline{E}_z^s=E_z^s(1+\mathrm{j}\eta_z^s)$	$\underline{E}_z^H=E_z^H(1+\mathrm{j}\eta_z^H)$
Shear modulus in the xy-plane	$\underline{G}_{xy}^c=G_{xy}^c(1+\mathrm{j}\eta_{xy}^c)$	$\underline{G}_{xy}^s=G_{xy}^s(1+\mathrm{j}\eta_{xy}^s)$	$\underline{G}_{xy}^H=G_{xy}^H(1+\mathrm{j}\eta_{xy}^H)$
Poisson ratio in the xy-plane	$\underline{\nu}_{xy}^c=\nu_{xy}^c(1+\mathrm{j}\eta_{\nu_{xy}}^c)$	$\underline{\nu}_{xy}^s=\nu_{xy}^s(1+\mathrm{j}\eta_{\nu_{xy}}^s)$	$\underline{\nu}_{xy}^H=\nu_{xy}^H(1+\mathrm{j}\eta_{\nu_{xy}}^H)$
Shear modulus in the xz-plane	$\underline{G}_{xz}^c=G_{xz}^c(1+\mathrm{j}\eta_{xz}^c)$	$\underline{G}_{xz}^s=G_{xz}^s(1+\mathrm{j}\eta_{xz}^s)$	$\underline{G}_{xz}^H=G_{xz}^H(1+\mathrm{j}\eta_{xz}^H)$
Poisson ratio in the xz-plane	$\underline{\nu}_{xz}^c=\nu_{xz}^c(1+\mathrm{j}\eta_{\nu_{xz}}^c)$	$\underline{\nu}_{xz}^s=\nu_{xz}^s(1+\mathrm{j}\eta_{\nu_{xz}}^s)$	$\underline{\nu}_{xz}^H=\nu_{xz}^H(1+\mathrm{j}\eta_{\nu_{xz}}^H)$
Shear modulus in the yz-plane	$\underline{G}_{yz}^c=G_{yz}^c(1+\mathrm{j}\eta_{yz}^c)$	$\underline{G}_{yz}^s=G_{yz}^s(1+\mathrm{j}\eta_{yz}^s)$	$\underline{G}_{yz}^H=G_{yz}^H(1+\mathrm{j}\eta_{yz}^H)$
Poisson ratio in the yz-plane	$\underline{\nu}_{yz}^c=\nu_{yz}^c(1+\mathrm{j}\eta_{\nu_{yz}}^c)$	$\underline{\nu}_{yz}^s=\nu_{yz}^s(1+\mathrm{j}\eta_{\nu_{yz}}^s)$	$\underline{\nu}_{yz}^H=\nu_{yz}^H(1+\mathrm{j}\eta_{\nu_{yz}}^H)$

The expressions of $\{u_k^n\}_{k\in[1,6]}$ are

$$\begin{cases} u_1^n = \dfrac{l_y}{2l_x}\sum_{l,m} M_{lm}^n \left[\sum_{p=0}^{N} M_{pm}^n J(l,p)\right] \\ u_2^n = \dfrac{1}{2}\sum_{l,m} M_{lm}^n \left[\sum_{p,q} N_{pq}^n I(l,p) I(lq)\right] \\ u_3^n = \dfrac{l_x}{2l_y}\sum_{l,m} N_{ml}^n \left[\sum_{p=0}^{N} N_{lp}^n J(m,p)\right] \\ u_4^n = \dfrac{l_x l_y}{8}\sum_{l,m}(N_{ml}^n)^2 - \dfrac{l_x}{2}\sum_{l,m} N_{ml}^n \left[\sum_{p=0}^{N} L_{lp}^n I(p,m)\right] + \dfrac{l_x}{2l_y}\sum_{l,m} L_{ml}^n \left[\sum_{p=0}^{N} L_{lp}^n J(m,p)\right] \\ u_5^n = \dfrac{l_x l_y}{8}\sum_{l,m}(M_{ml}^n)^2 - \dfrac{l_y}{2}\sum_{l,m} M_{ml}^n \left[\sum_{p=0}^{N} L_{pm}^n I(p,l)\right] + \dfrac{l_y}{2l_x}\sum_{l,m} L_{ml}^n \left[\sum_{p=0}^{N} L_{pm}^n J(l,p)\right] \\ u_6^n = \dfrac{l_x}{2l_y}\sum_{l,m} M_{ml}^n \left[\sum_{p=0}^{N} M_{lp}^n J(m,p)\right] + \sum_{l,m} M_{ml}^n \left[\sum_{p,q} N_{pq}^n I(p,l) I(m,q)\right] + \dfrac{l_y}{2l_x}\sum_{l,m} N_{ml}^n \left[\sum_{p=0}^{N} N_{pm}^n J(l,p)\right] \end{cases} \tag{C.2}$$

where the $I(l,p)$ and $J(l,p)$ are defined at the end of Appendix B.

Appendix D. Nomenclature

See Tables D1–D4.

Table D3
Notations used in the dynamical model of the panels.

$u(x,y,z)$ (m)	Displacement in the x-direction
$v(x,y,z)$ (m)	Displacement in the y-direction
$w(x,y,z)$ (m)	Displacement in the z-direction
$\Phi_x(x,y)$ (rad)	Rotation around the x-axis (Reissner–Mindlin hypothesis)
$\Phi_y(x,y)$ (rad)	Rotation around the y-axis (Reissner–Mindlin hypothesis)
$w_0(x,y)$ (m)	Displacement in the z-direction (Reissner–Mindlin hypothesis)
U (J)	Potential energy
ΔU (J)	Energy lost per cycle
T (J)	Kinetic energy
$D_1 = \dfrac{E_x^H h^3}{12(1-\nu_{xy}\nu_{yx})}$ (N m)	Plate rigidity in the x-direction
$D_2 = \dfrac{\nu_{xy} E_y^H h^3}{6(1-\nu_{xy}\nu_{yx})}$ (N m)	Plate rigidity in the xy-plane
$D_3 = \dfrac{E_y^H h^3}{12(1-\nu_{xy}\nu_{yx})}$ (N m)	Plate rigidity in the y-direction
$D_4 = 2\kappa_{yz}^2 h G_{yz}^H$ (N m)	Plate rigidity in the yz-plane
$D_5 = 2\kappa_{xz}^2 h G_{xz}^H$ (N m)	Plate rigidity in the xz-plane
$D_6 = \dfrac{G_{xy}^H h^3}{6}$ (N m)	Plate rigidity in the xy-plane
κ_{xz} (dimensionless)	Shear correction factor in the xz-plane
κ_{yz} (dimensionless)	Shear correction factor in the yz-plane
$\eta_\nu^{c,s,H} = \eta_{\nu_{xy}}^{c,s,H} + \eta_y^{c,s,H} = \eta_{\nu_{yx}}^{c,s,H} + \eta_x^{c,s,H}$ (dimensionless)	Global loss factor due to the Poisson ratio effects in the xy-plane
$\eta_1 = \eta_x^H$ (dimensionless)	Loss factor in the x-direction
$\eta_2 = \eta_\nu^H$ (dimensionless)	Global loss factor due to the Poisson ratio effects in the xy-plane
$\eta_3 = \eta_y^H$ (dimensionless)	Loss factor in the y-direction
$\eta_4 = \eta_{yz}^H$ (dimensionless)	Loss factor in the yz-plane
$\eta_5 = \eta_{xz}^H$ (dimensionless)	Loss factor in the xz-plane
$\eta_6 = \eta_{xy}^H$ (dimensionless)	Loss factor in the xy-plane
f (Hz)	Frequency
$\omega = 2\pi f$ (rad s^{-1})	Angular frequency
λ (m)	Wavelength of the flexural vibrations
$\lambda_x^{\min}$ (m)	Minimal wavelength of the flexural vibrations in the x-direction in the frequency range under study
$\lambda_y^{\min}$ (m)	Minimal wavelength of the flexural vibrations in the y-direction in the frequency range under study

Table D4
Notations used in the numerical model of the panels.

$\boldsymbol{K}$ (N m^{-1})	Stiffness matrix
$\boldsymbol{M}$ (kg)	Mass matrix
$\boldsymbol{C}$ (N m^{-1} s^{-1})	Damping matrix
f_n^{XP} (Hz)	Experimentally obtained modal frequency of the nth-mode
α_n^{XP} (s^{-1})	Experimentally obtained modal damping of the nth-mode
A_n^{XP} (s^{-1})	Experimentally obtained modal amplitude of the nth-mode
ϕ_n^{XP} (s^{-1})	Experimentally obtained modal phase of the nth-mode
f_n^{Num} (Hz)	Numerically obtained modal frequency of the nth-mode
α_n^{Num} (s^{-1})	Numerically obtained modal damping of the nth-mode
ξ_n^{Num} (m)	Numerically obtained modal shape of the nth-mode
μ (dimensionless)	Modal overlap
$\mathcal{P}_C$ (dimensionless)	Conservative system associated to the plate
f_n^C (Hz)	Modal frequency of the nth-mode of $\mathcal{P}_C$
ξ_n^C (Hz)	Modal shape of the nth-mode of $\mathcal{P}_C$
U_n^C (J)	Potential energy of the nth-mode of $\mathcal{P}_C$
T_n^C (J)	Kinetic energy of the nth-mode of $\mathcal{P}_C$
$\mathcal{P}_{NC}$ (dimensionless)	Non-conservative system associated to the plate
f_n^{NC} (Hz)	Modal frequency of the nth-mode of $\mathcal{P}_{NC}$
α_n (Hz)	Modal damping of the nth-mode of $\mathcal{P}_{NC}$
ξ_n^{NC} (Hz)	Modal shape of the nth-mode of $\mathcal{P}_{NC}$
U_n^{NC} (J)	Potential energy of the nth-mode of $\mathcal{P}_{NC}$
T_n^{NC} (J)	Kinetic energy of the nth-mode of $\mathcal{P}_{NC}$
ΔU_n^{NC} (J)	Energy lost per cycle by the nth-mode of $\mathcal{P}_{NC}$
Q (dimensionless)	Order of the polynomial basis (Rayleigh–Ritz procedure)
N (dimensionless)	Number of modes retained in the analysis
$p_i(x)$ (dimensionless)	ith element of the polynomial basis in the x-direction (Rayleigh–Ritz procedure)
$p_j(y)$ (dimensionless)	jth element of the polynomial basis in the y-direction (Rayleigh–Ritz procedure)
L_{ij} (rad)	Coordinates of $\Phi_x(x,y)$ in the polynomial basis (Rayleigh–Ritz procedure)
M_{ij} (rad)	Coordinates of $\Phi_y(x,y)$ in the polynomial basis (Rayleigh–Ritz procedure)
N_{ij} (m)	Coordinates of $w_0(x,y)$ in the polynomial basis (Rayleigh–Ritz procedure)

References

[1] E.O. Ayorinde, L. Yu, On the elastic characterization of composite plates with vibration data, *Journal of Sound and Vibration* 283 (1–2) (2005) 243–262.
[2] T. Lauwagie, H. Sol, W. Heylen, Handling uncertainties in mixed numerical–experimental techniques for vibration based material identification, *Journal of Sound and Vibration* 291 (3–5) (2006) 723–739.
[3] L.R. Deobald, R.F. Gibson, Determination of elastic-constants of orthotropic plates by a modal-analysis Rayleigh–Ritz technique, *Journal of Sound and Vibration* 124 (2) (1988) 269–283.
[4] F. Moussu, M. Nivoit, Determination of elastic-constants of orthotropic plates by a modal-analysis method of superposition, *Journal of Sound and Vibration* 165 (1) (1993) 149–163.
[5] M. Grediac, N. Fournier, P.A. Paris, Y. Surrel, Direct identification of elastic constants of anisotropic plates by modal analysis: experimental results, *Journal of Sound and Vibration* 210 (5) (1998) 643–659.
[6] S.F. Hwang, C.S. Chang, Determination of elastic constants of materials by vibration testing, *Composite Structures* 49 (2) (2000) 183–190.
[7] K.G. Muthurajan, K. Sanakaranarayanasamy, B.N. Rao, Evaluation of elastic constants of specially orthotropic through vibration testing, *Journal of Sound and Vibration* 272 (1–2) (2004) 413–424.
[8] C.M.M. Soares, M.M. Defreitas, A.L. Araujo, P. Pederson, Identification of material properties of composite plate specimens, *Composite Structures* 25 (1–4) (1993) 277–285.
[9] A.L. Araujo, C.M.M. Soares, M.J.M. deFreitas, Characterization of material parameters of composite plate specimens using optimization and experimental vibrational data, *Composites Part B—Engineering* 27 (2) (1996) 185–191.
[10] E.O. Ayorinde, Elastic constants of thick orthotropic composite plates, *Journal of Composite Materials* 29 (8,15) (1995) 1025–1039.
[11] T.C. Lai, K.H. Ip, Parameter estimation of orthotropic plates by Bayesian sensitivity analysis, *Composite Structures* 34 (1) (1996) 29–42.
[12] P.S. Frederiksen, Experimental procedure and results for the identification of elastic constants of thick orthotropic plates, *Journal of Composite Materials* 31 (4) (1997) 360–382.
[13] P.S. Frederiksen, Numerical studies for the identification of orthotropic elastic constants of thick plates, *European Journal of Mechanics A—Solids* 16 (1) (1997) 117–140.
[14] P.S. Frederiksen, Application of an improved model for the identification of material parameters, *Mechanics of Composite Materials and Structures* 4 (4) (1997) 297–316.
[15] P.S. Frederiksen, Parameter uncertainty and design of optimal experiments for the estimation of elastic constants, *International Journal of Solids and Structures* 35 (12) (1998) 1241–1260.
[16] A.K. Bledzki, A. Kessler, R. Rikards, A. Chate, Determination of elastic constants of glass/epoxy unidirectional laminates by the vibration testing of plates, *Composites Science and Technology* 59 (13) (1999) 2015–2024.
[17] J. Cunha, J. Piranda, Application of model updating techniques in dynamics for the identification of elastic constants of composite materials, *Composites Part B—Engineering* 30 (1) (1999) 79–85.
[18] A.L. Araujo, C.M.M. Soares, M.J.M. de Freitas, P. Pedersen, J. Herskovits, Combined numerical–experimental model for the identification of mechanical properties of laminated structures, *Composite Structures* 50 (4) (2000) 363–372.
[19] S. Gagneja, R.F. Gibson, E.O. Ayorinde, Design of test specimens for the determination of elastic through-thickness shear properties of thick composites from measured modal vibration frequencies, *Composites Science and Technology* 61 (5) (2001) 679–687.
[20] J. Cugnoni, T. Gmur, A. Schorderet, Identification by modal analysis of composite structures modelled with FSDT and HSDT laminated shell finite elements, *Composites Part A—Applied Science and Manufacturing* 35 (7–8) (2004) 977–987.

[21] J. Cugnoni, T. Gmur, A. Schorderet, Inverse method based on modal analysis for characterizing the constitutive properties of thick composite plates, *Computers & Structures* 85 (17–18) (2007) 1310–1320.
[22] M.E. McIntyre, J. Woodhouse, On measuring the elastic and damping constants of orthotropic sheet materials, *Acta Metallurgica* 36 (6) (1988) 1397–1416.
[23] J. de Visscher, H. Sol, W.P. de Wilde, J. Vantomme, Identification of the damping properties of orthotropic composite materials using a mixed numerical experimental method, *Applied Composite Materials* 4 (1) (1997) 13–33.
[24] J.P. Talbot, J. Woodhouse, The vibration damping of laminated plates, *Composites Part A—Applied Science and Manufacturing* 28 (12) (1997) 1007–1012.
[25] G.L. Qian, S.V. Hoa, X.R. Xiao, A vibration method for measuring mechanical properties of composite, theory and experiment, *Composite Structures* 39 (1–2) (1997) 31–38.
[26] E. Pagnacco, A. Moreau, D. Lemosse, Inverse strategies for the identification of elastic and viscoelastic material parameters using full-field measurements, *Materials Science and Engineering A—Structural Materials Properties Microstructure and Processing* 452 (April) (2007) 737–745.
[27] M. Matter, T. Gmur, J. Cugnoni, A. Schorderet, Numerical–experimental identification of the elastic and damping properties in composite plates, *Composite Structures* 90 (2) (2009) 180–187.
[28] A. Giraudeau, F. Pierron, B.Q. Guo, An alternative to modal analysis for material stiffness and damping identification from vibrating plates, *Journal of Sound and Vibration* 329 (10) (2010) 1653–1672.
[29] A.L. Araujo, C.M.M. Soares, J. Herskovits, P. Pedersen, Estimation of piezoelastic and viscoelastic properties in laminated structures, *Composite Structures* 87 (2) (2009) 168–174.
[30] T. Saito, R.D. Parbery, S. Okuno, S. Kawano, Parameter identification for aluminum honeycomb sandwich panels based on orthotropic Timoshenko beam theory, *Journal of Sound and Vibration* 208 (2) (1997) 271–287.
[31] Y.M. Shi, H. Sol, H.X. Hua, Material parameter identification of sandwich beams by an inverse method, *Journal of Sound and Vibration* 290 (3–5) (2006) 1234–1255.
[32] N. Barbieri, R. Barbieri, L.C. Winikes, Parameters estimation of sandwich beam model with rigid polyurethane foam core, *Mechanical Systems and Signal Processing* 24 (2) (2010) 406–415.
[33] S.F. Bastos, L. Borges, F.A. Rochinha, Numerical and experimental approach for identifying elastic parameters in sandwich plates, *Shock and Vibration* 9 (4–5) (2002) 193–201.
[34] M.N. Ichchou, O. Bareille, J. Berthaut, Identification of effective sandwich structural properties via an inverse wave approach, *Engineering Structures* 30 (10) (2008) 2591–2604.
[35] J. Berthaut, M.N. Ichchou, L. Jezequel, Piano soundboard: structural behavior, numerical and experimental study in the modal range, *Applied Acoustics* 64 (11) (2003) 1113–1136.
[36] M. Matter, T. Gmur, J. Cugnoni, A. Schorderet, Identification of the elastic and damping properties in sandwich structures with a low core-to-skin stiffness ratio, *Composite Structures* 93 (2) (2011) 331–341.
[37] E. Barkanov, E. Skukis, B. Petitjean, Characterisation of viscoelastic layers in sandwich panels via an inverse technique, *Journal of Sound and Vibration* 327 (3–5) (2009) 402–412.
[38] A.L. Araujo, C.M.M. Soares, C.A.M. Soares, J. Herskovits, Characterisation by inverse techniques of elastic, viscoelastic and piezoelectric properties of anisotropic sandwich adaptive structures, *Applied Composite Materials* 17 (5) (2010) 543–556.
[39] W.S. Burton, A.K. Noor, Assessment of continuum models for sandwich panel honeycomb cores, *Computer Methods in Applied Mechanics and Engineering* 145 (3–4) (1997) 341–360.
[40] K. Ege, X. Boutillon, B. David, High-resolution modal analysis, *Journal of Sound and Vibration* 325 (4–5) (2009) 852–869.
[41] S.D. Yu, W.L. Cleghorn, Free flexural vibration analysis of symmetric honeycomb panels, *Journal of Sound and Vibration* 284 (1–2) (2005) 189–204.
[42] Q.L. Liu, Y. Zhao, Natural frequency analysis of a sandwich panel with soft core based on a refined shear deformation model, *Composite Structures* 72 (3) (2006) 364–374.
[43] J.S. Kim, Free vibration of laminated and sandwich plates using enhanced plate theories, *Journal of Sound and Vibration* 308 (1–2) (2007) 268–286.
[44] C.E. Wallace, Radiation-resistance of a rectangular panel, *Journal of the Acoustical Society of America* 51 (3) (1972) 946–&.
[45] A. Chaigne, C. Lambourg, Time-domain simulation of damped impacted plates. i. Theory and experiments, *Journal of the Acoustical Society of America* 109 (4) (2001) 1422–1432.
[46] T. Pritz, Frequency dependences of complex moduli and complex Poisson's ratio of real solid materials, *Journal of Sound and Vibration* 214 (1) (1998) 83–104.
[47] G.B. Muravskii, On frequency independent damping, *Journal of Sound and Vibration* 274 (3–5) (2004) 653–668.
[48] E. Nilsson, A.C. Nilsson, Prediction and measurement of some dynamic properties of sandwich structures with honeycomb and foam cores, *Journal of Sound and Vibration* 251 (3) (2002) 409–430.
[49] L. Cremer, M. Heckl, B.A.T. Peterson, *Structure-Borne Sound: Structural Vibrations and Sound Radiation at Audio Frequencies*, third ed., Springer-Verlag, 2005.
[50] V. Birman, On the choice of shear correction factor in sandwich structures, *Journal of Sandwich Structures & Materials* 4 (1) (2002) 83–95.
[51] M. Geradin, D. Rixen, *Mechanical Vibrations*: *Theory and Applications to Structural Dynamics*, 1997.
[52] F. Cortes, M.J. Elejabarrieta, An approximate numerical method for the complex eigenproblem in systems characterised by a structural damping matrix, *Journal of Sound and Vibration* 296 (1–2) (2006) 166–182.
[53] C.D. Johnson, D.A. Kienholz, Finite-element prediction of damping in structures with constrained viscoelastic layers, *AIAA Journal* 20 (9) (1982) 1284–1290.
[54] P.J. Torvik, B. Runyon, Modifications to the method of modal strain energy for improved estimates of loss factors for damped structures, *Shock and Vibration* 14 (5) (2007) 339–353.
[55] R.B. Bhat, Natural frequencies of rectangular-plates using characteristic orthogonal polynomials in Rayleigh–Ritz method, *Journal of Sound and Vibration* 102 (4) (1985) 493–499.
[56] C.S. Kim, Natural frequencies of rectangular-plates using characteristic orthogonal polynomials in Rayleigh–Ritz method—comment, *Journal of Sound and Vibration* 108 (1) (1986) 166–168.
[57] M. Rébillat, R. Hennequin, E. Corteel, B.F.G. Katz, Prediction of harmonic distortion generated by electro-dynamic loudspeakers using cascade of Hammerstein models, in: *128th Convention of the Audio Engineering Society*, 2010.
[58] M. Rébillat, R. Hennequin, E. Corteel, B.F.G. Katz, Identification of cascade of Hammerstein models for the description of nonlinearities in vibrating devices, *Journal of Sound and Vibration* 330 (2011) 1018–1038.
[59] R. Roy, T. Kailath, Esprit—estimation of signal parameters via rotational invariance techniques, *IEEE Transactions on Acoustics Speech and Signal Processing* 37 (7) (1989) 984–995.
[60] R. Badeau, B. David, G. Richard, A new perturbation analysis for signal enumeration in rotational invariance techniques, *IEEE Transactions on Signal Processing* 54 (2) (2006) 450–458.
[61] J. Laroche, The use of the matrix pencil method for the spectrum analysis of musical signals, *Journal of the Acoustical Society of America* 94 (4) (1993) 1958–1965.
[62] C.T. Kelley, *Iterative Methods for Optimization*, Society for Industrial and Applied Mathematics, Philadelphia, 1999.
[63] L.J. Gibson, M.F. Ashby, *Cellular Solids: Structure and Properties*, second ed., Cambridge University Press, 2001.

[64] P. Verpeaux, T. Charras, A. Millard, Castem 2000: une approche moderne du calcul des structures, *Calcul des structures et intelligence artificielle* (1988) 261–271.
[65] J.C. Lagarias, J.A. Reeds, M.H. Wright, P.E. Wright, Convergence properties of the Nelder–Mead simplex method in low dimensions, *SIAM Journal of Optimization* 9 (1998) 112–147.
[66] A.L. Araujo, C.M. Mota Soares, J. Herskovits, P. Pedersen, Visco-piezo-elastic parameter estimation in laminated plate structures, *Inverse Problems in Science and Engineering* 17 (2) (2009) 145–157.